VILNIUS UNIVERSITY

IEVA ŠAKINYTĖ

REAGENTLESS ENZYMATIC SYSTEMS CONSISTING OF
CARBONACEOUS STRUCTURES

Summary of doctoral dissertation

Physical science, biochemistry (04 P)

Vilnius, 2017

This work was carried out at the Vilnius University, Life Sciences Center, Institute of Biochemistry, Department of Bioanalysis during 2012 – 2016.

Scientific supervisor:

Dr. Julija Razumienė (Vilnius University, physical sciences, biochemistry – 04 P).

Scientific consultant:

Prof. habil. dr. Jurgis Barkauskas (Vilnius University, physical sciences, chemistry – 03 P).

The dissertation is defended at the Concil of Biochemistry science direction of Vilnius University:

Chairman:

Prof. habil. dr. Albertas Malinauskas (Center for Physical Sciences and Technology, physical sciences, chemistry – 03 P).

Members:

Dr. Žilvinas Anusevičius (Vilnius University, physical sciences, biochemistry – 04 P),

Dr. Justas Barauskas (Malmö University, Sweden, physical sciences, biochemistry – 04 P),

Prof. dr. Rasa Pauliukaitė (Center for Physical Sciences and Technology, physical sciences, chemistry – 03 P),

Doc. dr. Gintaras Valinčius (Vilnius University, physical sciences, biochemistry – 04 P).

The defence of doctoral dissertation will take place on April 20th, 2017, at 11:00 a. m. at the public meeting of Council at Auditorium (R-402) of Vilnius University, Life Sciences Center.

Address: Saulėtekio av. 7, LT – 10257 Vilnius, Lithuania.

Summary of the dissertation has been sent out on 20th March, 2017.

The dissertation is available at the Library of Vilnius University and at official Vilnius University website: http://www.vu.lt/naujienos/ivykiu-kalendorius

VILNIAUS UNIVERSITETAS

IEVA ŠAKINYTĖ

BEREAGENTINĖS FERMENTINĖS SISTEMOS ANGLINIŲ STRUKTŪRŲ PAGRINDU

Daktaro disertacijs santrauka,

Fiziniai mokslai, biochemija (04 P)

Vilnius, 2017

Disertacija rengta 2012 – 2016 metais Vilniaus universiteto Gyvybės mokslų centro Biochemijos instituto Bioanalizės skyriuje.

Mokslinė vadovė:

Dr. Julija Razumienė (Vilniaus universitetas, fiziniai mokslai, biochemija – 04 P).

Mokslinis konsultantas:

Prof. habil. dr. Jurgis Barkauskas (Vilniaus universitetas, fiziniai mokslai, chemija – 03 P).

Disertacija ginama Vilniaus universiteto Biochemijos mokslo krypties taryboje:

Pirmininkas:

Prof. habil. dr. Albertas Malinauskas (Fizinių ir technologijos mokslų centras, fiziniai mokslai, chemija – 03 P).

Nariai:

Dr. Žilvinas Anusevičius (Vilniaus universitetas, fiziniai mokslai, biochemija – 04 P),
Dr. Justas Barauskas (Malmö universitetas, Švedija, fiziniai mokslai, biochemija – 04 P),
Prof. dr. Rasa Pauliukaitė (Fizinių ir technologijos mokslų centras, fiziniai mokslai, chemija – 03 P),
Doc. dr. Gintaras Valinčius (Vilniaus universitetas, fiziniai mokslai, biochemija – 04 P).

Disertacija bus ginama viešame Biochemijos mokslo krypties tarybos posėdyje 2017 m. balandžio menesio 20 d. 11:00 val. Vilniaus universiteto, Gyvybės mokslų centre (LT-10257 Vilnius, Saulėtekio al. 7) R-402 auditorijoje.

Disertacijos santrauka išsiuntinėta 2017 kovo mėnesio 20 d.

Disertacija galima peržiūrėti Vilniaus universiteto bibliotekoje ir VU internetinėje svetainėje adresu: http://www.vu.lt/naujienos/ivykiu-kalendorius

INTRODUCTION

In the current age of technology, in the scientific research field, the creation of heterogeneous enzymatic bioanalytic and bioconversion systems takes an important place, because they can be used for obtaining of desired products or to detect concern analytes in more efficient and cheaper way. The creation of those systems is a quite challenging process, because not all the enzymes and the materials of different phase are compatible with each other. Moreover, the enzymes are short living components and usually their regeneration is complicated, because their active sites are usually deeply embedded in the protein globule [1, 2].

Immobilizing of oxidoreductases or other electrochemically active product formatting enzymes on suitable materials (electrodes), not only extends their living period, bus also facilitates or even ensures the regeneration of these enzymes. Moreover, due to this, between enzyme active site and electrode surface direct electron transport (DET) can be achieved, this process is the base of reagentless systems [3]. Such reagentless electrochemical systems are highly selective; therefore, they are promising in the creation of amperometric biosensors. Amperometric biosensors offer a promising alternative for the conventional methods (e.g. potentiometric or spectrophotometric). They have great potential because of their high sensitivity and selectivity, easier instrumentation, rapid (real-time) detection, low cost and ability to be used in turbid fluids [3, 4]. Due to these properties, reagentless amperometric biosensors are promising in development of simple and portable equipment for medical diagnostics, environmental and industrial process monitoring [5, 6].

Aiming to create effective reagentless amperometric biosensors, the main attention should be paid to the selection of appropriate electrode material, which would be suitable for effective bioelectrocatalytic processes. Due to unique physical and electrochemical properties, sp^2 hybridized carbonaceous materials have a unique place in the creation field of such systems [7 – 9]. Graphene can be considered as an ideal electrode material because of its large theoretical surface area (2630 $m^2 \cdot g^{-1}$), superior electrical conductance (64 $mS \cdot cm^{-1}$), large potential window and fast electron transfer rate [10]. Moreover, the presence of oxygen containing groups on graphene surface can enhance electron transfer rate between electrode surface and enzyme active site [11] or cause DET [12]. One of the

most commonly-used methods to prepare the graphene based materials with oxygen containing groups on their surface is the chemical oxidation of graphite.

The aim of this study was to synthesize, select and characterize sp^2 hybridized carbonaceous materials, which would be suitable for development of effective reagentless enzymatic systems. The samples of carbonaceous materials have been synthesized by four different oxidation protocols and by using thermal reduction of Hummers and Offeman's method obtained graphite oxide and graphene oxide [13]. The characteristics of newly synthesized carbonaceous materials were evaluated using thermal gravimetric analysis, atomic force microscopy, Brunauer-Emmett-Teller, scanning electron microscope, X-ray diffraction, Raman spectroscopy, titrimetric and elemental analysis. The obtained carbonaceous materials have been tested as electrode materials applicable in amperometric biosensors using soluble pyrroloquinoline quinone dependent glucose dehydrogenase from *Acinetobacter calcoaceticus* sp., urease from *Canavalia ensiformis* or D-fructose dehydrogenase from *Gluconobacter industrius*. The most effective biosensors were selected for carbamide measurements in dialysate of hemodialysis patients and D-tagatose detection in D-galactose bioconversion into D-tagatose reaction mixture.

The aim of this work was to synthesize, select and characterize the sp^2 hybridized carbonaceous materials and to use them for creation of highly effective reagentless enzymatic systems.

The objectives:

1. To synthesize graphite and graphene oxides, different graphite oxidation products and thermally reduced graphite oxide. To design optimized method which would allow to synthesize the different fractions of thermally reduced graphene oxide possessing defined properties;

2. To characterize the synthesized materials by titrimetric, atomic force microscopy, Raman spectroscopy, Brunauer-Emmett-Teller, thermal gravimetric, scanning electron microscopy, X-ray diffraction and elemental analysis methods;

3. To apply the synthesized and characterized carbonaceous materials for design of reagentless systems based on pyrroloquinoline quinone dependent glucose dehydrogenase from *Acinetobacter calcoaceticus* sp., urease from *Canavalia ensiformis* or D-fructose dehydrogenase from *Gluconobacter industrius*. To characterise these systems by main kinetic parameters;

6

4. After evaluation of systems main kinetic characteristics, to select the appropriate carbonaceous materials for design of D-glucose, carbamide and D-fructose reagentless biosensors. To characterise the biosensors by main characteristics;

5. To select and apply the reagentless carbamide and D-fructose biosensors for analysis of real samples.

The novelty and significance of the work

1. For the first time it is shown that for successful synthesis of GOPs graphite oxidation in alkaline media with H_2O_2 or $K_3[Fe(CN)_6]$ and enzyme laccase from *Coriolopsis byrsina*were can be used. DET between active sites of PQQ-GDH and GOPs or TRGrO based electrode surface was achieved. The DET determining properties of GOPs and TRGrO were established.

2. The proposed vertical thermal reduction and fractionalization system of GO allowed us to collect three different fractions of TRGO with defined properties. These fractions of TRGO are applicable for design of high efficiency reagentless D-fructose and carbamide biosensors. The efficiency of these biosensors is comparable to synergistic mediated processes. The systems efficiency and stability determining properties of TRGO fractions were established.

3. It has been shown that the second TRGO fraction and urease based biosensor is suitable for precise and direct detection of carbamide in dialysate of hemodialysis patients, while the first TRGO fraction and immobilized FDH based biosensor is suitable for amperometric reagentless D-fructose detection and precise detection of D-tagatose in D-galactose bioconversion reaction mixture.

Approbation of the research result. The result of the research were presented in 9 scientific publication, 6 of them as articles have been published in the jornal included into Thomson Reuters Web of science data base. The research results have been presented in 2 Lithuanians national and 15 international scientific conferences.

Structure of the dissertation. The doctoral dissertation is written in Lithuanian and consists of the introduction, literature review, experimental, results and discussion, conclusions, the list of references (191 references) and the list of orginal scientific publications. The material of the doctoral dissertation is presented in 133 pages, including 47 figures and 15 tables.

2 EXPERIMENTAL

2.1 Enzymes

Soluble pyrroloquinoline quinone-dependent glucose dehydrogenase (PQQ-GDH) from *Acinetobacter calcoaceticus* sp. L.M.D. 79.41 (E.C.1.1.5.2) was purified according to the known protocol [14] (Department of Molecular microbiology and biotechnology VU GMC Institute of Biochemistry); urease from *Canavalia ensiformis* (E.C. 3.5.1.5.) (Sigma, USA); D-fructose dehydrogenase from *Gluconobacter industrius* (EC 1.1.99.11) (FDH) (Sigma, USA); Laccase from *Coriolopsis byrsina* EC. 1.10.3.2 was separated according to the protocol [15] (Department of Molecular microbiology and biotechnology, VU GMC Institute of Biochemistry); termophilic L-arabinose isomerase (TAI) from *Geobacillus lithuanicus 52 (*TAI) (Department of Molecular microbiology and biotechnology, VU GMC Institute of Biochemistry).

2.3 Synthesis of sp^2 hybridized carbonaceous materials

2.3.1 Synthesis of graphite and graphene oxide

Graphite oxide (**GrO**) was synthesized using the protocol proposed by Hummers and Offeman ($KMnO_4$ and $NaNO_3$ in concentrated H_2SO_4) [13]. According to this protocol 2.5 g of $NaNO_3$ and 5 g of graphite powder was gradually put into 115 ml of concentrated H_2SO_4 by keeping temperature of 20 °C. After that 15 g of $KMnO_4$ was added gradually under stirring and the temperature of the mixture was kept below 22 °C. After all operations, the mixture was stirred at 35 °C for 30 min and then carefully diluted with 230 ml of distilled H_2O. After that concentrated (30%) H_2O_2 was added into the mixture until the total volume of 700 ml. The slurry was filtered and further decanted with H_2O aiming to remove the acidity of the filtrate until the neutral pH. Further GO particles were dried for one day under atmospheric conditions and successively for one weak in a vacuum.

Graphene oxide (**GO**) was synthesized from the natural graphite according to the protocol reported by Yan et al. [17]. In a typical experiment, graphite powder was treated with 24 mL conc. H_2SO_4, 5 g $K_2S_2O_8$ and 5 g P_2O_5 at 80 °C for 4.5 h. Then, this pre-oxidized graphite was subjected to oxidation by Hummer's method [18]. Afterwards the GO particles were washed with distilled water by centrifugation (5500 rpm; each run for 20 min) several times until the pH of the filtrate was neutral. Obtained brown powder was dried in desiccator to a constant weight.

2.3.2 Synthesis of graphite oxidation products

Graphite oxidation products (**GOP1** and **GOP2**) have been prepared by carrying out the synthesis in the alkaline media. Two types of pristine graphite powder: as-purchased, and sonified have been treated with concentrated H_2O_2 under temperature not exceeding 0 °C during 3 weeks. Firstly, 50 ml of saturated KOH solution in H_2O_2 was prepared under stirring and cooling and 5 g of graphite was added into this solution gradually under stirring and the temperature of the mixture was kept below 5 °C. Secondly, the mixture was kept at 0 °C for 3 weeks. Further the reaction mixture was decanted and rewashed with distilled water until the pH revived neutral. Then the powder was dried under atmospheric conditions. Two types of the graphite GOP1 and GOP2 have been obtained by proposed protocol accordingly to the pristine graphite powder: as-purchased or sonified.

Graphite oxidation products (**GOP3** and **GOP4**) have been prepared by treating two types of pristine graphite powder: as-purchased and sonified with $K_3[Fe(CN)_6]$ in alkaline media for 3 weeks not exceeding 0 °C. Firstly, 50 ml of saturated KOH aqueous solution was prepared under stirring and cooling and then 5 g of the graphite was added into this solution gradually. The reaction mixture was chilled up to °0 C and 15 g of $K_3[Fe(CN)_6]$ was added into this solution. Further the mixture was kept below 5 °C for 3 weeks and finally, the reaction product was decanted and rewashed with distilled water until the pH revived neutral. Finally, the powder was dried under atmospheric conditions. Two types of the graphite GOP3 and GOP4 have been obtained by proposed protocol accordingly to the pristine graphite powder (as-purchased or sonified) were used.

Graphite oxidation product (**GOP5**) has been prepared by using the enzyme laccase from *Coriolopsis byrsina* (7000 U/ml) in alkaline media. For this case 14 mg of graphite powder were mixed with 10 µl of the laccase and 10 µl of phosphate buffer solution (pH 4.2) and the reaction mixture was kept for 24 h at 15 ºC. Further the mixture was decanted up to neutral medium and reaction product was dried for 5 min under 50 ℃.

2.3.3 Thermal reduction of graphite and graphene oxide

Thermal reduction of GrO. Thermally reduced graphite oxide (**TRGrO**) sample was obtained by reduction of GrO. According to this protocol 5 g of the GrO were kept in stream of argon (60 ml/min) for 1 h in horizontal furnace centre. Further GO was heated in stream of argon (30 ml/min) under 800 – 900 ºC for 1 h and chilled to the room temperature.

Thermal reduction and fractionation of **GO** was performed using the equipment shown in Fig. 1. 1.0 g of dry GO powder crushed in an agate mortar has been added to the separator funnel (Fig. 1; 5) and sealed.
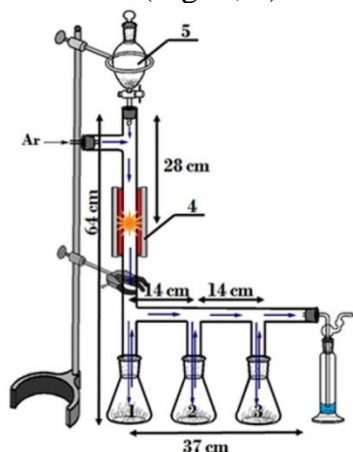

Fig. 2. 1 *Equipment used for the thermal reduction and fractionation of GO. 1 - chamber for TRGO1, 2 - chamber for TRGO2, 3 - chamber for TRGO3, 4 - heating zone, and 5 - separatory funnel for GO.*

Ar was passed through the system during 1 h; Ar flow rate was maintained at 60.0 ml/min. After 1 h the furnace (Fig. 1; 4) was heated up to 800 °C and GO powder from the sealed separator funnel has been subjected to the hot zone in small portions (~0.05 g). During this part of the experiment the Ar flow rate was maintained at 100.0 ml/min. Thermally reduced GO particles are moved away from the hot reaction zone by the Ar flow and settle in subsequent chambers (Figs. 1; 1, 2 and 3) depending on the charge and mass. Collected fractions of reduced GO are labeled as TRGO1, TRGO2 and TRGO3, respectively. The mass ratio of TRGO1 : TRGO2 : TRGO3 in the experiment was obtained as 0.428 : 0.019 : 0.004, respectively.

2.4 Characterization methods of sp^2 hybridized carbonaceous materials

Thermal gravimetric analysis (TGA). TGA measurements were carried out using thermal gravimetric analysis equipment (Pyris 1, Clarus 600 T MS Perkin-Elmer, USA). The measurements of 10 mg of each carbonaceous materials sample were performed in temperature range of 25 $^{\circ}$C – 500 $^{\circ}$C at a scan rate of 10 $^{\circ}$C·min^{-1} under nitrogen atmosphere.

Raman spectroscopy. Raman spectra were obtained on a confocal Raman spectrometer/microscope (LabRam HR800, Horiba JobinYvon, USA). A 633 nm He-Ne laser was used as the excitation source. The laser power at the sample was restricted to 1 mW and the laser beam was focused to 2 μm diameter spot on the surface. Spectra were taken with the 50x objective lens. The overall integration time was 100 s. Frequencies and intensities of Raman bands were determined by fitting the experimental contour with Gaussian-Lorentzian components.

Brunauer–Emmett–Teller (BET) analysis has been applied for all carbonaceous materials powders by using BET analyzer (TriStar II 3020, Micromeritics, USA). The N_2 adsorption and desorption isotherms were measured at –196 $^{\circ}$C. Prior to the gas sorption measurements, all the samples were outgassed in N_2 atmosphere at 100 $^{\circ}$C for 2 h. The specific surface area was calculated using the BET method.

Titration of functional groups. The amount of acidic and basic functional groups on the surface of GOPs and GrO samples was determined titrimetrically using 0.1 M and 0.01 M solutions of NaOH, Na_2CO_3, $NaHCO_3$ or HCl according ref. [19].

AFM measurement. Surfaces of prepared samples using all GOPs were analyzed by scanning probe microscope (D3100/Nanoscope IVa, Veeco Instruments Inc., USA). Tapping mode of surface scanning was used for visualization and characterization of the particles. The data and AFM images were processed by the NanoScope Software 6.14 (Veeco Instruments Inc.). The samples for AFM measurements have been prepared as follows. Firstly, the aqueous suspensions of carbonaceous materials were obtained by mixing of 0.5 mg powder of GOP with 120 μl of distilled water. 10 μl of the suspension were dropped onto silica plate and dried under 110 $^{\circ}$C for 10 min and then left in a ventilating hood until the sample temperature decreases up to 30 $^{\circ}$C. Aiming to reduce moisture of the sample surface before each measurement the samples were additionally dried under 50 $^{\circ}$C for 20 min.

Scanning electron microscope (SEM) images were obtained using a Hitachi SU-70 scanning electron microscope at an accelerating voltage of 5.0 kV at magnifications of 25,000–100,000×. SEM images of GO were generated using a 0.8 kV deceleration voltage.

The bulk density was determined by weighting and volume measurement of powder samples [20].

Elemental analysis was performed using a Thermo Scientific FLASH 2000 Series CHNS/O Analyzer. Carbonaceous materials samples were weighed (20 mg) and introduced into the pyrolysis chamber (1060 °C). Produced oxygen contained gases were captured in a mixing chamber and homogenized before being separated using gas chromatography with thermal conductivity detection. High purity helium was used as carrier gas. The results were reported as percent by weight of oxygen.

X-ray diffraction (XRD) studies were performed using an X-ray diffractometer Bruker D8 Advance with Cu Kα radiation ($K_{\alpha 1} = 1.54056$ Å). XRD of the powder samples was recorded for 2θ values from 10° to 55°. The characterization was done at 40 keV and 40 mA with a step size of 0.040° and a dwell time of 1.0 s.

2.5 Preparation of biosensors and electrochemical measurements

Aiming to design working electrodes, carbonaceous materials were extruded by forming tablet. The tablet was sealed in a Teflon tube with amorphous carbon pasta. Electrodes were washed with bi-distilled water, and dried before use. Working electrode (biosensor) was designed by adsorbtion or mechanically attaching and fixing the membrane containing immobilized enzyme to the surface of the electrode. The basic scheme of biosensor construction is presented in Figure 1.
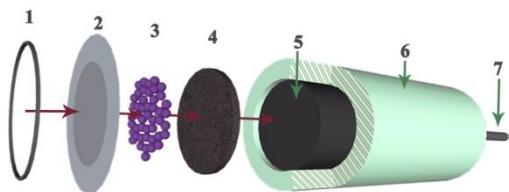
Fig. 2.2 *Basic scheme of the amperometric biosensor: 1 - rubber ring, 2 - terylene film, 3 - layer of enzyme, 4 - electrode layer consisting of carbonaceous material, 5 - electrode contact zone, 6 - corps, 7 - electrical wire.*

Chronoamperometry measurements were performed using an electrochemical system (PARSTAT 2273, Princeton Applied Research, USA) with a conventional three-electrode system comprised of a platinum plate electrode as auxiliary, a saturated Ag/AgCl electrode as reference and working electrodes using carbonaceous materials (biosensor). The response of the prepared biosensors to the addition of enzyme substrate was investigated under potentiostatic conditions (the following conditions are considered as standard for each system): at +0.4 V in a stirred 0.05 M acetate buffer solution, pH 6.0 in a case of PQQ-GDH; at +0,2 V in a stirred 0.02 M phosphate buffer solution, pH 7.2 in a case of urease; at +0.4 V in a stirred McIlvaine, pH 4.5, and K-phosphate buffer, pH 7.5 buffer solutions. All measuremens were obtained at 20 ºC temperature.

From the experimental dependence of the current density (j) on substrate concentration (C), the apparent maximum response density (j_{max}^{app}) and apparent Michaelis constant (K_M^{app}) were evaluated. For this, the response curent density was measured three times in the solution with C and the average response j was obtained. The experimental dependence j vs. C was approximated by OriginPro 8 (free trial version from http://www.originlab.com, OriginLab Corporation, USA) according to the electrochemical version of the Michaelis-Menten Eq [21]. (1):

$$ j = \frac{j_{max}^{app}\,[S]}{K_M^{app} + [S]} \tag{1} $$

The j_{max}^{app} is maximal oxidation current density generated by bioelectrocatalytic process (describes effectiveness of biosensor) and K_M^{app} is apparent Michaelis constant which is a key technical characteristic of the amperometric biosensor. K_M^{app} represents the linearity [22] of the calibration curve and qualitatively characterizes the biosensor as a reaction-diffusion system: when the apparent Michaelis constant is much larger than its value for soluble enzyme Michaelis constant (K_M), it means that significant diffusion barrier is present between the sample and the reaction layer [23, 24].

Sensitivity of the biosensors were defined as a slope of the linear range of calibration curve.

Detection limit (LOD) was calculated as the standard deviation of the current of response to substrate (in the linear calibration curve range) multiplied by three and divided by the sensitivity [25].

The inactivation constants (k_{in}) were calculated for biosensors as a slope obtained in semi-logarithmic coordinates of amperometric responses to substrate (in linear calibration curve range) vs. time.

2.5.1 Enzyme immobilization

The **PQQ-GDH** was immobilized on 2 mm diametre individual flexible support of 0.1% (2 µl) PVA coated terylene film. Adsorption of 2 µl (18000 U·ml^{-1}) of PQQ-GDH at room temperature to the support was the method for the immobilization of the enzyme. The biosensor was designed by mechanically attaching and fixing with rubber ring the membrane, containing immobilized PQQ-GDH to the surface of the electrode consisting of different carbonaceous materials: GOPs, GrO, TRGrO and graphite.

The **urease** was immobilized on the flexible support of terylene pre-coated with 0.1% (2 µl) PVA by cross linking of 2 µl of urease (2 mg/30 µl (80 kU·g^{-1}) in phosphate buffer solution (pH 7.2) containing 2 mg of BSA) using 5 µl of 5% glutaraldehyde. The biosensor was designed by mechanically attaching and fixing with rubber ring the membrane, containing immobilized urease to the surface of the electrode consisting of different carbonaceous materials: GOPs, GrO, GO,TRGrO, TRGO fractions or graphite.

FDH immobilization. D-fructose biosensor was prepared by the adsorption on the electrode surface consisting of different carbonaceous materials (GO, TRGO fractions or graphite). of 2 µl, 0.5% triton X-100 solution in water (30 min, 10 °C). Then 2 µl of FDH (1471 U·ml^{-1}) in McIlvaine buffer solution (pH 4.5) were absorbed for 30 min, at 10 °C. Finally, the biosensor was designed by mechanically attaching and fixing the flexible terylene film with rubber ring to the pretreated surface of the electrode.

3 RESULTS AND DISCUSSION

3.1 Examination of sp^2 hybridized carbonaceous materials

3.1.1 Examination of GOPs and TRGrO

Aiming to evaluate amount and type of oxygen functional groups of newly synthesized GOPs and GrO, the titration method was applied [19]. Results are given in Table 3.1.

Table 3.1 *Functional groups determined on the surface of GrO and GOP samples.*

Samples	Amount of acidic functional groups, mmol·g^{-1}			Amount of basic functional groups mmol·g^{-1}
	Hydroxy-	Carboxy-	Lactone	
GrO	3.433	1.511	0.278	0.000
GOP1	0.000	0.000	0.000	0.108
GOP2	0.000	0.000	0.000	0.157
GOP3	0.000	0.000	0.000	0.138
GOP4	0.000	0.000	0.000	0.167
GOP5	–	–	–	–
TRGrO	–	–	–	–
Graphite	0.000	0.000	0.000	0.000

Acidic functional groups (hydroxy-, carboxy- and lactone) are present in GrO samples in the quantities, which are considerably less in comparison with total oxygen at the C : O ratio 2.7 : 1 [26]. Consequently, the largest amount of oxygen in GrO should be

incorporated into the basal plane of graphene, most probably, in the form of epoxy groups. No acidic functional groups have been found in the all GOPs samples; they can be characterized by presence of the basic functional groups. For the samples obtained from the sonified graphite raw material amount of the basic functional groups is higher in comparison with the samples from as-purchased graphite.

The presence of oxygen functional groups on a surface of all synthesized carbonaceous materials was approved by the thermal gravimetric analysis (TGA). TGA is a reliable analytical technique based on measurements of the weight loss of materials as a function of temperature. The core of the method is that the investigated samples lose the weight as they are heated from a simple process such as drying or from chemical reactions or decompositions that liberate gases [27]. The TGA curves of all carbonaceous materials and the pristine graphite are shown in Figure 3.1 A.
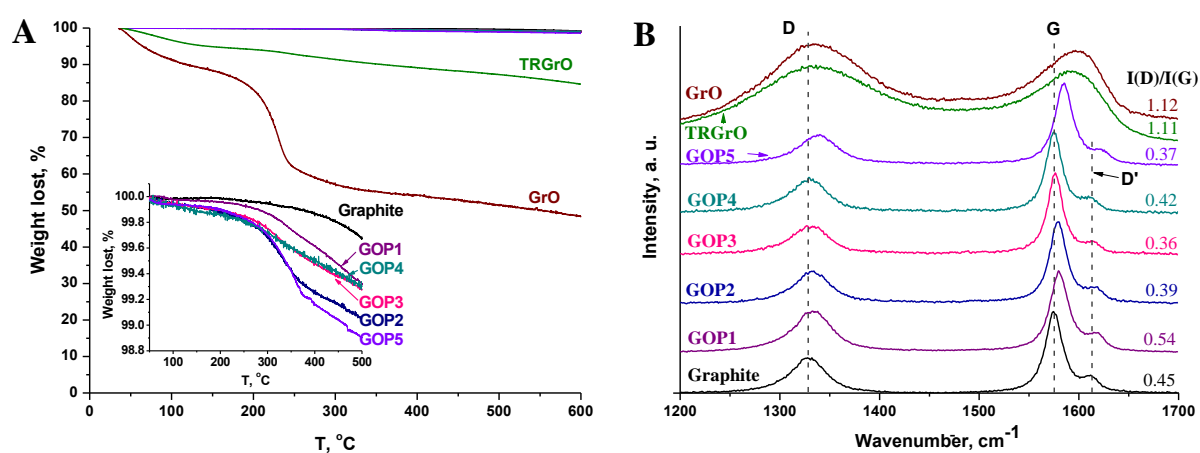

Fig. 3.1 *TGA data (A) and Raman spectra (B) of graphite, GrO, GOPs and TRGrO.*

As it can be clearly seen in Fig. 3.1, the samples differ in their thermal behavior. Pristine graphite displays rather simple linear dependence, without any steps, indicating a uniform weight loss probably of adsorbed impurities. In contrast, the TGA curve of GrO showed two distinct steps: the weight loss from 25 to 150 °C is due to the evaporation of water (12 %) [27], the second one from 150 to 400 °C (34 %) is caused by decomposition of labile oxygen groups (carboxylic, lactone or anhydride) [27, 28]. The TGA curves of GOPs in the first step do not showed pronounced weight loss, whereas the weight loss of TRGrO was up to 5 %. In the temperature range of 150 – 400 °C where the weight loss of carbonaceous materials occurs due to the changes in their chemical structure: elimination of labile functional groups and by forming of CO_2 or CO [27, 28] the TGA curves of GOP1, GOP2, GOP3, GOP4 ir GOP5 shows approximately 1 % of the weight loss, TRGrO

– 6 % whereas pristine graphite did not exhibited any changes in TGA curve. These data confirms the presence of oxygen functionalities on the surface of GOPs. The thermal treatment of GrO under inert atmosphere also produced TRGrO with some basic character [28]. The lower amount of acidic functional groups of TRGrO compared to GrO confirms that the surfaces of this product became more hydrophobic.

Aiming to study newly synthesized GrO, GOPs and TRGrO Raman spectroscopy was applied because the Raman spectroscopy is known as a powerful technique in characterization of carbon structures [29]. The G band is the most significant attribute in the Raman spectra of sp^2 hybridized carbon materials. Another band called D band indicates a certain amount of disorder of edges within the carbon structure [30]. The G band of carbonaceous materials has E_{2g} symmetry. Its eigenvector involves the in-plane bond-stretching motion of pairs of carbon sp^2 atoms. This mode does not require the presence of sixfold rings. D and D′ – disorder induced bands that are observed in defective structures. The D band is a breathing mode of A_{1g} symmetry. This mode is forbidden in perfect graphite and only becomes active in the presence of disorder. The D mode is strictly connected to the presence of sixfold aromatic ring. Due to defects on graphene sheets its structure becomes not so tight like in graphite and symmetric vibration of sixfold aromatic rings expressed as D band intensity (I(D)) increases [31, 32]. D and G band intensity (I(D)/I(G)) ratio show the level of disorder in graphene. D′ is the double resonance Raman process generated band and presents the graphite edge imperfection [31, 32]. In this study Raman spectra of all carbonaceous materials were performed in the range of $1200 – 1700$ cm^{-1} and are presented in Fig. 3.1 B.

As it is clearly seen in Fig. 3.1 B, Raman spectra of GrO and TRGrO differs from other GOPs because these spectra exhibit only presence of D and G peaks, whereas all spectra of GOPs are rather similar to pristine graphite. The Raman spectrum of the pristine graphite shows a high intensity G peak at 1575 cm^{-1}, a D peak at 1328 cm^{-1} and a weak D′ peak at 1612 cm^{-1}. The GOPs G, D and D′ bands compared to the pristine graphite G band are shifted to higher wavenumber area (blue shift). The blue shift occurs mostly due to the isolated double bonds, which are formed during the oxidation process [26, 31, 33]. The largest blue shift is obtained for the GrO samples (20.6 cm^{-1}), supposedly it occurs due to the formation of large amount of oxygen containing functional groups that originates the isolated double bonds in the reaction with strong oxidizing agents (KMnO$_4$,

NaNO$_3$, H$_2$SO$_4$). In the case of graphite treated with weak oxidants (H$_2$O$_2$, K$_3$[Fe(CN)$_6$]), small amount of oxygen containing functional groups is formed (products labeled as GOP1, GOP2, GOP3 and GOP4). Thus, the blue shift in the spectra of GOP1, GOP2, GOP3 and GOP4 are negligible: for GOP1 and GOP2 it is ~5 cm^{-1} and for GOP3 and GOP4 it is ~1 cm^{-1}. In fact, H$_2$O$_2$ has stronger oxidizing properties (redox potential is 0.878 V [34]) than K$_3$[Fe(CN)$_6$] (redox potential is 0.486 V [35]) in strong solution of alkalis. Therefore, we assume that H$_2$O$_2$ oxidizes not only the higher reactivity carbon atoms at the edges of the graphene sheets; some of basal plane atoms, which are lower in reactivity, are also oxidized forming isolated double bonds. Whereas, K$_3$[Fe(CN)$_6$] has apparently weaker oxidizing properties and reacts with the carbon atoms at the edges exclusively. In the case of enzymatically oxidized GOP5, the blue shift of G peak is 10 cm^{-1}. We still do not know exactly the mechanism of the enzymatic oxidation, but it is most likely that laccase due to its spatial positioning is able catalytically oxidize basal carbon atoms rather these at the edges. Therefore, this is the reason of the large blue shift of G peak indicating the appearance of the isolated double bonds.

Compared the peak of G band of GrO to that of TRGrO, the peak of TRGrO is more closely shifted toward the position of the G band in graphite. It shows that part of sp^2 bonding network during the process of thermal reduction was restored [33]. However, during the process of removal of oxygen functional groups from GrO, vacancies and topological defects are formed inside the graphene planes. Furthermore, during the oxidation of graphite, as well as the reduction of GrO, the amorphization of graphite takes place by resulting in transition of sp^2 bonds to sp^3 [26]. Due to the amorphization of graphite the intensity ratio of D and G band (I(D)/I(G)) increases [31, 33]. The I(D)/I(G) ratios of GOP1, GOP2, GOP3, GOP4 and GOP5 do not significantly differ from that of pristine graphite (Fig. 3.1 A). These data suggest that during the oxidation process the amorphization of graphite does not take place. On the contrary, the samples GOP2, GOP3, GOP4 and GOP5 are characterized by the lower concentration of defects compared to that in pristine graphite. The ratio I(D)/I(G) values of GrO and TRGrO are obtained of 1.12 and 1.11, respectively and this is more than two times higher than that of pristine graphite (0.45). This is the evidence that during the oxidation the graphite amorphization takes place yielding small and disordered particles.

The GrO, GOPs, TRGrO and graphite particles were examined and characterized by AFM. Two-dimensional representation of AFM topographic data of graphite and GOPs is shown in Fig. 3.2 All samples were characterized by parameters such as average particle diametre (d_{av}) and the average particle height (h_{av}). The average diameter of particles and the average particle height are summarized in Table 3.2.
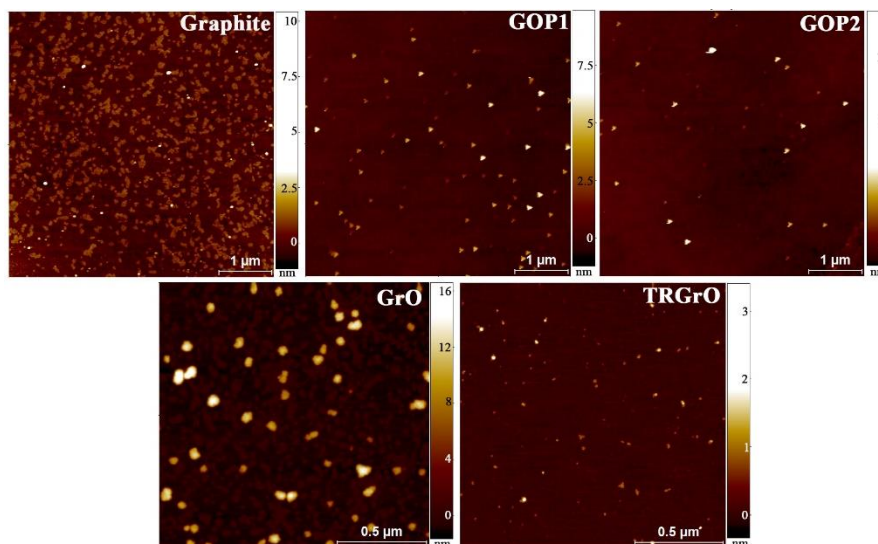

Fig. 3.2 *Two-dimensional AFM images of the graphite, GOP1, GOP2, GrO and TRGrO.*

Table 3.2 *Physical properties of graphite, GrO, TRGrO and GOPs determined by AJM and BET analysis.*

Material	d_{av}, nm	h_{av}, nm	S_{BET}, $m^2 \cdot g^{-1}$
GrO	26	0.95	59.9 ± 0.6
	52	8	
GOP1	48	2.6	8.1 ± 0.03
GOP2	53	3.4	8.7 ± 0.03
GOP3	62	5.5	8.2 ± 0.04
GOP4	50	3.5	10.1 ± 0.06
GOP5	56	1.8	7.6 ± 0.06
TRGrO	11	0.5	235.8 ± 1.1
Graphite	76	1.3	13.1 ± 0.04

The AFM data clearly show that all synthesized carbonaceous materials are composed of nanometric particles ($d_{vid.}$ are from 11 to 62 nm and $h_{vid.}$ from 0.5 to 5.5 nm). The TRGrO particles have the smallest size while the GOP3 particles have the biggest size (Fig. 3.2 and Table 3.2).

Comparing d_{av} of pristine graphite to that of GOPs, it can be concluded that the oxidation process is able to reduce the diameter of the particle. However, average height of GOP1, GOP2, GOOP3, GOP4, GOP5 and GrO is higher than that of graphite. This could be due to the interaction of oxygen function groups in GOPs samples with those on the silica plates during the drying process. In the case of GrO, two sets of the particles with different sizes were obtained. Average diameter of large particles was ~52 nm and average

height was ~8 nm, while average diameter of small particles was ~26 nm and average height was ~1 nm. The obtained average height of small particles coincides with that reported for the single layer of graphene oxide [36]. The measured average diameter of TRGrO particles was ~11 nm and the average particle height was ~0.5 nm, which is very close to that of the single layer of graphene (0.39 nm) [37].

The specific surface area (S_{BET}) of all samples was evaluated using the Brunauer–Emmett–Teller (BET) method. All synthesized carbonaceous materials S_{BET} were obtained from the N_2 adsorption-desorption isotherms. It was found that all N_2 adsorption-desorption isotherms of samples are characterized by an H3 hysteresis loop, which is typical for plate-like particles [28, 39]. This fact was confirmed by the AFM data (Fig. 3.2 and Table 3.2): all materials have a diameter between 26 and 76 nm and a height between 0.5 and 5.5 nm. These AFM date approved the flat (plate-like) nature of the graphite, GrO, TRGrO and GOPs particles. The BET data are shown in Table 3.2.

The S_{BET} of oxidation products GOP1, GOP2, GOP3, GOP4 and GOP5 was lower than that of pristine graphite. For GOP2 and GOP4, where sonified pristine graphite was used in the oxidation procedure, insignificantly higher S_{BET} of oxidized products were found compared to GOP1 and GOP3 respectively. In fact, this was expected because according to Guittonneau et al. [40] during the sonication the amorphization of graphite occurred. Decrease of S_{BET} for GOP1, GOP2, GOP3, GOP4 and GOP5 compared to that of pristine graphite, is most likely due to the interactions between oxygen-containing functional groups at the edges, which are able to form closed structures that lower surface areas. The surface area of TRGrO compared to that of GrO was increased more than four times during the reduction process. Moreover, TRGrO S_{BET} was increased eighteen times compared to that of graphite and almost twenty five times compared to the others of GOPs.

3.1.2 Examination of TRGO fractions

Proposed vertical thermal reduction system allowed us to separate and collect three different fractions of TRGO (TRGO1, TRGO2 and TRGO3) with different physicochemical properties. Since the nature and quantity of surface functional groups and other surface characteristics of graphene materials have a great influence on the work of a biosensor, three different fractions of TRGO were thoroughly characterized by SEM, TGA, XRD, Raman spectroscopy and BET measurements.

17

Aiming to evaluate amount of oxygen functional groups of newly synthesized TRGO fractions and GO, the TGA and elemental analysis method were applied. Results are given in Figure 3.3. TGA curves of newly synthesized carbonaceous materials show a weight loss between 35 °C and 500 °C.
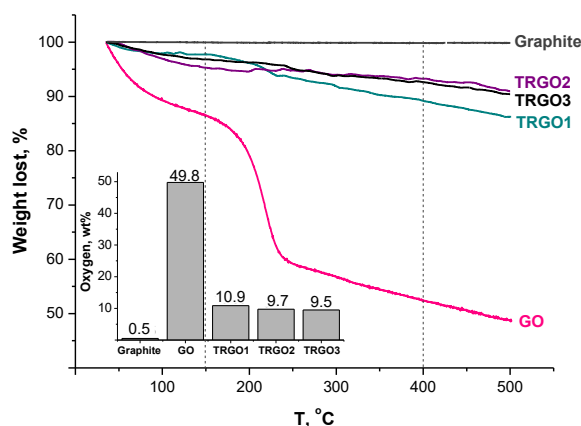

Fig. 3.3 *Data of TGA and elemental analysis (inset) of graphite, GO and TRGO fractions.*

Up to 150 °C the weight loss occurs due to the removal of water (in the form of adsorbed moisture and intercalated H_2O) [27]. Maximal values in this interval are reached for GO (13%); for TRGO fractions this parameter is significantly less (up to 5%), and no weight loss for graphite is observed. In the temperature interval 150 – 400 °C weight loss of carbonaceous materials occurs due to the changes in their chemical structure: elimination of labile functional groups (carboxy, lactone, epoxy, phenolic) in the form of CO_2 or CO [28]. The most pronounced weight loss is for the GO (34%) and TRGO1 (8%) samples. The maximum rate this process reaches at c.a. 275 °C for both types of carbonaceous materials; the circumstance which proves the similarity of the processes that occur in both materials. Supposedly, remains of GO structure in the TRGO1 fraction are responsible for the similarities of both processes. The mass change for TRGO2 and TRGO3 occurs evenly in the temperature interval 150 - 500 °C; so, we can conclude that these fractions include less oxygen-containing functional groups in comparison with these in TRGO1. This conclusion is consistent with the data obtained from elemental analysis (see inset in Fig. 3.3).

SEM images of graphite GO and TRGO fractions are shown in Fig. 3.4 a - e. The sites with typical morphology features are shown in insets at higher magnification.
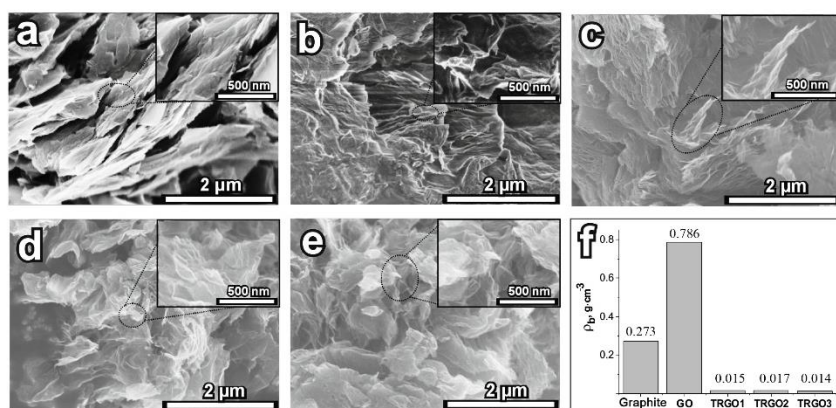
18

Fig. 3.4 *SEM images of graphite (a), GO (b), TRGO1 (c), TRGO2 (d) and TRGO3 (e). Bulk densities of graphite, GO and TRGO fractions (f).*

The characteristic change of morphology during the process of thermal reduction of GO is observed. In the case of graphite, crystalline lamellar structure is clearly visible. Much less crystallinity is observed in GO, nevertheless, the structure of GO should be considered to be compact. The SEM results also show the change in morphology of TRGO fractions. Graphene layers in the case of TRGO fractions are stacked in a random fashion, with turbostratic defects. The thermal reduction is accompanied by a pronounced decrease in the structure compactness; bulk density (ρ_b) data of graphite, GO and TRGO fractions are presented in Figure 3.4 f. ρ_b data are consistent with the SEM results: decrease in the ρ_b of TRGO fractions is associated with a random distribution of separate graphene sheets. The XRD patterns of graphite, GO and TRGO fractions are presented in Fig. 3.5 A.
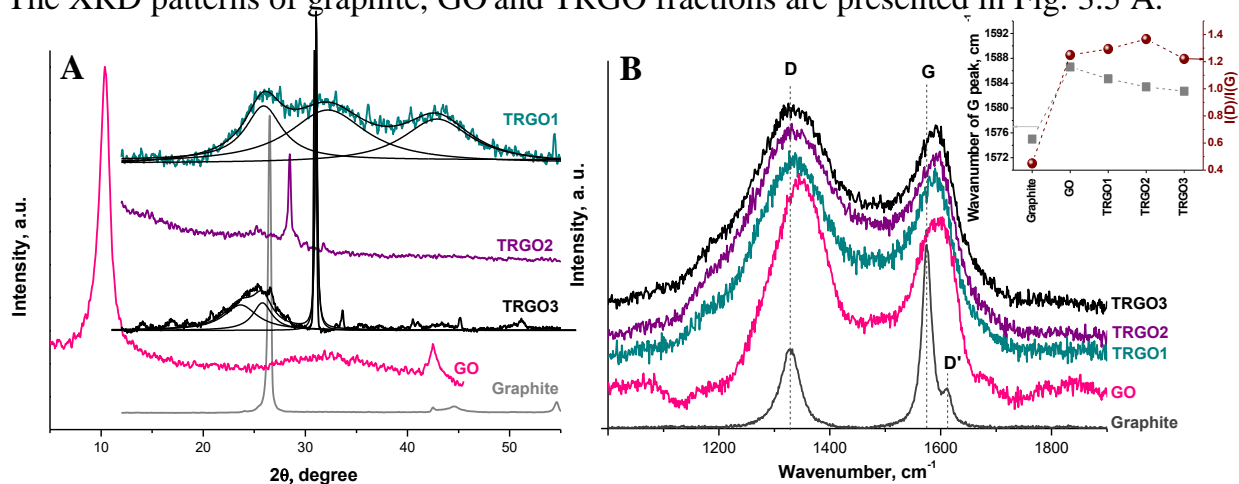

Fig. 3.5 *XRD data (supplemented with fitting curves) (A) and Raman spectra (excitation wavelength 633 nm) of graphite, GO and TRGO fractions, the inset shows the G peak position and intensity ratio I(D)/I(G) (B).*

The XRD pattern of graphite is compared to that in the PDF card 00-056-0159. A sharp peak at $2\theta = 26.54°$ (002) and less intensive peaks at $2\theta = 42.36°$ (100), $2\theta = 44.56°$ (101) and $2\theta = 55.66°$ (004) are present in the diffractogram of graphite. The interlayer distance d_{002} in graphite powder samples determined from the peak at 26.54° equals 0.34

nm; the crystallite size reaches a value of about 31.9 nm. The peaks in the diffractogram of GO ($2\theta = 10.35°$ and $2\theta = 42.57°$) correspond to the enlarged interlayer distance of 0.86 nm and the crystallite size of 7.2 nm. The XRD patterns of TRGO fractions indicate that certain ordered structure exists in the case of TRGO2 and TRGO3, while amorphous structure prevails in the case of TRGO1. At this point, we do not have the complete information to explain the origin of pronounced crystalline structures in the TRGO2 and TRGO3 fractions. The peaks of crystalline phase in XRD patterns of TRGO2 and TRGO3 ($2\theta = 28.49°$ and $2\theta = 30.95°$ respectively) do not coincide with those of pure graphite and GO. In both cases the peaks are shifted to higher angles indicating the contraction of the interlayer distance (0.31 nm for TRGO2 and 0.29 nm for TRGO3).

Raman spectra of graphite, GO and TRGO fractions in the range of $1000 - 1900$ cm^{-1} are shown in Fig. 3.5 B. Two peaks (D and G) are dominant in the spectra of all samples.

The Raman spectrum of the pristine graphite shows a G peak of high intensity at 1575 cm^{-1}, a D peak at 1328 cm^{-1}, and a weak D' peak at 1612 cm^{-1}. The G band in GO is shifted 12 cm^{-1} to higher frequencies compared to the pristine graphite (Fig. 3.5 B inset). We suggest that this shift is mostly affected by the isolated double bonds in the structure of GO, which resonate at higher frequencies [31]. In TRGO fractions the positions of G band are shifted slightly to the values more close to that of pristine graphite (Fig. 3.5 B inset) indicating that in-plane sp^2 bonding network was restored during the thermal reduction process. In TRGO3 the position of G band is shifted mostly due to this TRGO3 is consist of mostly reduced particles with less amount of oxygen groups. Thermal reduction of GO involves the removal of oxygen containing functional groups, thus creating defects within the graphene basal plane. Additionally, it has been suggested that TRGO fractions exhibit a mixture of sp^2 and sp^3 bonds that depends on the degree of reduction. Furthermore, the electrical transport behavior changes from insulator-hoping-like to semimetal-band-like as the number of localized π states increases [41]. D and G band intensity (I(D)/I(G)) ratio (Fig. 3.5 B inset) shows the level of disorder in graphene. According to this parameter, all TRGO fractions contain approximately the same amount of defects, while the highest concentration is present in TRGO2 (I(D)/I(G) = 1.4).

Specific surface area is one of the most important characteristics for graphene based materials. These materials with high surface area are promising candidates for biosensors [8, 42]. The S_{BET} and d_{av} of pore of all samples were evaluated using the BET method. The

data are shown in Table 3.3. The BET surface area data of graphite, GO and TRGO fractions were obtained from the N_2 adsorption-desorption isotherms. It was found that all isotherms of samples are characterized by an H3 hysteresis loop, which is typical for plate-like particles [38, 39].

Table 3.3 *BET data of graphite, GO and TGRO fractions.*

	S_{BET}, m²·g⁻¹	d_{av}, Å
Graphite	12.8 ± 0.1	107.9 ± 14.0
GO	11.1 ± 0.2	42.3 ± 5.5
TRGO1	316.8 ± 1.1	142.3 ± 18.5
TRGO2	689.5 ± 11.3	148.8 ± 19.3
TRGO3	503.0 ± 15.7	146.3 ± 19.0

Going from graphite to the thermally reduced fractions of GO, up to TRGO2, the S_{BET} and d_{av} of pore were increasing. The TRGO2 powder is characterized by the highest surface area (689.5 ± 11.3 m²·g⁻¹), however it is significantly lower than the theoretical surface area (2630 m²·g⁻¹) reported for an individual graphene sheet [43]. S_{BET} of TRGO2 was increased almost sixty times compared to that of GO and more than two times compared to that of TRGO1. The surface area and average pore width of TRGO3 were slightly smaller than that of TRGO2. As can be seen in Fig. 3.5 B (inset) the concentration of defects of TRGO3 is lower compared to that of TRGO2. This could explain the smaller S_{BET} of TRGO3.

It is known that during the oxidation process the graphite crystallites are reduced in size [26, 44]; simultaneously amount of defects is considerably increased (inset in Fig. 3.5 B). However, as can be seen in Table 3.3, S_{BET} and d_{av} of pore of GO have the smallest values. This divergence could be explained by the fact that the N_2 molecules are unable to penetrate the interlamellar space of GO [45].

3.2 Carbonaceous materials and enzymes based reagentless systems
3.2.1 Examination of PQQ – GDH based reagentless systems

To define the possible factors that might be resposible for successful ET in bioelectrocatalytic systems acting on a principle of DET, the biosensors using the synthesized carbonaceous materials and pristine graphite have been investigated on a base of glucose oxidation reactions catalyzed by pyrroloquinoline quinone-dependent glucose dehydrogenase (PQQ-GDH). In a case of control biosensor the, pristine graphite was used for electrode construction. The current response of the manufactured biosensors to D-glucose was measured as the difference between the steady state current and the

background current. The current density as a factor of the successful ET between the active site of the enzyme and the electrode surface (expressed as the maximal oxidation current (j_{max}^{app})) was calculated for each biosensor under saturating concentration of substrate. Both kinetic parameters of biosensors the j_{max}^{app} and the apparent Michaelis constant (K_M^{app}) were summarized in Fig. 3.6 A.
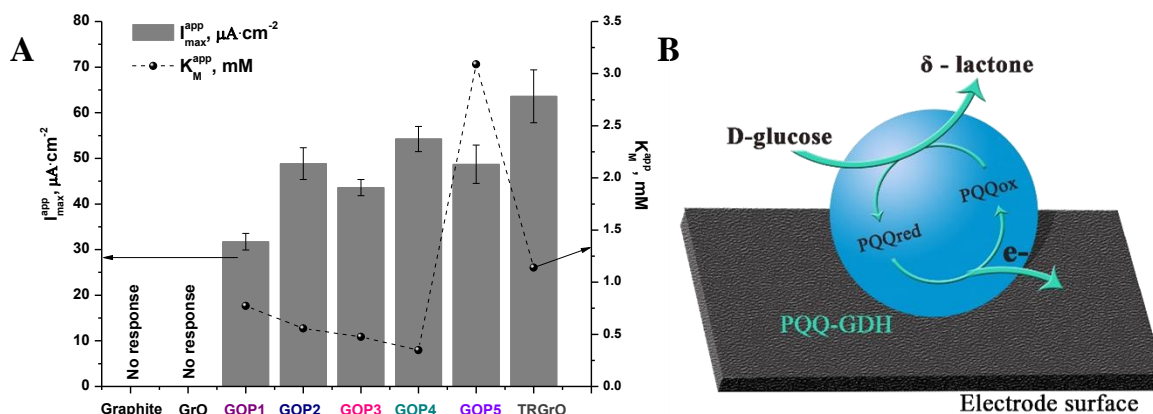

Fig. 3.6 *Kinetic characteristic of biosensors measured under standard conditions (A) and DET between active site of PQQ-GDH and electrode using GOPs and TRGrO, E = 0.4V vs. Ag/AgCl (B).*

As can be seen in Fig. 3.6 A, biosensors based on PQQ-GDH acting on electrodes using GrO or pristine graphite do not show any response to D-glucose, while j_{max}^{app} for others materials changed from 63.6 ± 5.8 to 31.7 ± 1.8 µA·cm^{-2} for TRGrO and GOP1, respectively. Different values of j_{max}^{app} obtained for all biosensors indicate that the slowest and limiting stage is the electron transfer from the enzyme active site to the electrode surface, rather than the ET from the substrate to the enzyme. On purpose to understand what factors defined the successful ET in such bioelectrocatalytic systems, the principle of direct bioelectrocatalysis has to be explored. Schematically, the involvement of the enzymes in the DET can be represented as shown in a case of PQQ-GDH in Fig. 3.6 B.

Obviously, ET to/from electrode can be provided exclusively by the enzymes catalyzing redox reactions. DET presumes an absence of any freely diffusing or even immobilized ET mediating compounds. Thus, electron has to be transferred directly from active site of enzyme to electrode surface (in a case of electrooxidation). However, the number of bioelectrocatalytic systems possessing DET are strongly restricted due to the nature of enzymes or distance between electrode surface and the active site of the enzyme. PQQ-GDH does not possess any intrinsic ET mediators (hemes). Thus, in absence of additional mediating materials, PQQ-GDH does not indicate any catalytic redox behavior

even on non pre-oxidized SWCNT electrode [46]. Thus, novel electrode materials allowing DET in enzymatic systems are still very actual.

Apparently, carbonaceous materials containing proper surface morphology or functionalities are very promising for amperometric biosensorics because it opens new possibilities to overcome ET restrictions in such systems. Considering the drastic differences of j_{max}^{app} source values of studied biosensors based on synthesized carbonaceous materials and titrimetric, TGA, BET, Raman spectroscopy and AFM analysis, it was highly interesting to understand, what parameters of GOPs and TRGrO were responsible for successful ET. TRGrO exhibited highest efficiency and by TGA analysis it could be matched to the high degree of oxygen functional groups, but in a case of GrO this degree is even higher, however, PQQ-GDH does not transfer electrons to the GrO electrode surface (Fig. 3.6 A). BET analysis also reveals higher surface area of TRGrO (235.8 ± 1.1 $m^2 \cdot g^{-1}$) suggesting that the highest ET acceleration in biosensor could be attributed only to this factor. However, GrO possess much higher surface area 59.9 ± 0.6 $m^2 \cdot g^{-1}$ compared to other GOPs ($7.6 \pm 0.06 - 10.08 \pm 0.06$ $m^2 \cdot g^{-1}$), but GrO are absolutely unusable for PQQ-GDH bioelectrocatalytic system working on a principle of DET. Moreover, efficiency of GOPs varied from 31.7 ± 1.8 to 54.3 ± 2.8 $\mu A \cdot cm^{-2}$ that is quite close to the efficiency of TGRrO, although surface area of these GOPs were at least $40 - 20$ times less than in a case of TRGrO. Obviously, TRGrO possess smallest sizes of particles that can be promising feature allowing proper ET distance. Also for successful ET in biosensors operating on DET mode the enzyme orientation is crucial [47, 48] thus, the absence of proper functionalities helps to orient the enzyme. TGA data revealed that TRGrO had oxygen functional groups that can serve for enzyme orientation. Although, examination of Raman spectra of the GrO and the TRGrO showed that for achieving of DET the carbonaceous material has to possess not only high degree of defects but also well π-conjugated bond system which defines excellent electrical conductivity and high electron mobility. To summarize, the efficiency of DET strongly depends on optimal functionalities, morphology (S_{BET}, d_{av}, h_{av}) and structural features (defectiveness) of carbonaceous materials.

It should be also noted, that the systems based on TRGrO and GOP5 exhibited higher K_M^{app} value compared to that of native enzyme (0.5 mM) [49] (Fig. 3.6 A). In fact, K_M^{app}

23

value in heterogeneous electro-catalytic systems depends on two parameters: shape of the active center affected during immobilization of the enzyme (that usually increases K_M^{app} values) and the substrate concentration onto electrode surface. In general, higher values of K_M^{app} as compared to values of native enzymes obtained in solution for majority of biosensors indicate that the slowest and limiting stages are the substrate diffusion to enzyme active site and the ET from the enzyme active site to the electrode surface. The samples obtained from the sonified graphite raw material (GOP2 and GOP4) exhibit lower K_M^{app} values in comparison with the samples obtained using as-purchased graphite raw material. This result may be explained by the facts that the GOPs obtained from the sonified graphite raw material (GOP2 and GOP4) have higher amount of basic functional groups and S_{BET} in comparison with the GOPs from as-purchased graphite (GOP1 and GOP3) (Table 3.1 and Table 3.2). These characteristics improved the affinity of PQQ-GDH to the electrode surface. For this reason, the K_M^{app} values of biosensor become lower. It also was observed that K_M^{app} values depend on the amount of defects of carbonaceous materials (Fig. 3.1 B).

The operational stability of the biosensors prepared with GOPs, TRGrO and PQQ-GDH was studied. For this, the continuous measurements of the responses at a working potential of 0.4 V for D-glucose (5 mM) were carried out in acetate buffer solution at least 800 h. The inactivation data of biosensors are presented in Figure 3.7 A. Inactivation constants (k_{in}) for D-glucose biosensors based on DET were calculated.
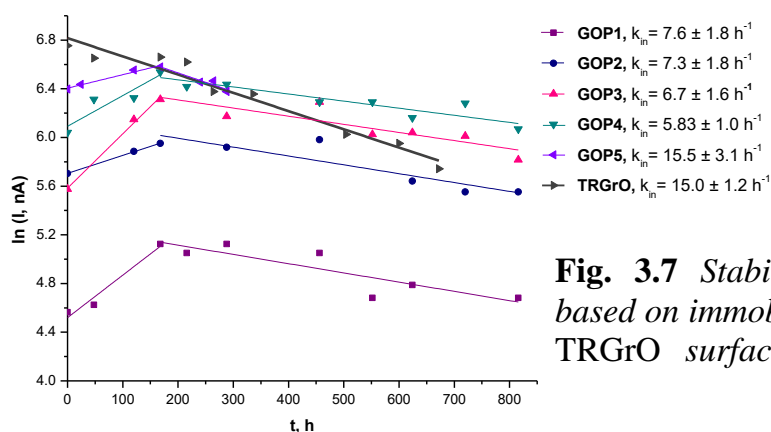

GOP1, k_{in} = 7.6 ± 1.8 h^{-1}
GOP2, k_{in} = 7.3 ± 1.8 h^{-1}
GOP3, k_{in} = 6.7 ± 1.6 h^{-1}
GOP4, k_{in} = 5.83 ± 1.0 h^{-1}
GOP5, k_{in} = 15.5 ± 3.1 h^{-1}
TRGrO, k_{in} = 15.0 ± 1.2 h^{-1}

Fig. 3.7 *Stability of D-glucose biosensors based on immobilized PQQ-GDH on* GOPs or TRGrO *surface measured under standard*

As can be seen in Fig. 3.7, the sensitivity of biosensors based on GOP1, GOP2, GOP3, GOP4 ir GOP5 increases during 168 h due to a reorganization of the matrix and an improvement of the contact and orientation between the PQQ-GDH globule and the carbonaceous materials electrodes. After a period of 168 h, the sensitivities of these

biosensors decrease linearly. Meanwhile, sensitivity of biosensors based on TRGrO decreases linearly from the first measurement. The calculated inactivation constants for different carbonaceous materialas based biosensors were 7.6 ± 1.8 h^{-1} (GOP1), 7.3 ± 1.8 h^{-1} (GOP2), 6.7 ± 1.6 h^{-1} (GOP3), 5.8 ± 1.0 h^{-1} (GOP4), 15.5 ± 3.1 h^{-1} (GOP5) and 15.0 ± 1.2 h^{-1} (TRGrO). It was found that k_{in} for biosensors based on GOP5 and TRGrO were higer comparing with others biosensors. The TGA and titrimetric analysis (Fig. 3.1 A and Table 3.1) revealed that the GOP5 and the TRGrO have the largest amount of the oxygen containing functional groups that participate in ET from the active site of the PQQ-GDH to the electrode. In our opinion, the sensitivity of biosensors were decreased due to oxygen containing functional groups reduction during the experimental period.

3.2.2 Examination of urease based reagentless systems

To define the main factors responsible for successful ET in bioelectrocatalytic systems acting on a principle of DET, the biosensors using all the synthesized carbonaceous materials (GOP1, GOP2, GOP3, GOP4, GOP5, GrO, GO, TRGrO, TRGO1, TRGO2 and TRGO3) and pristine graphite (control biosensor) have been investigated on a base of carbamide hydrolysis reactions catalysed by urease based biosensor. Urease catalyses the hydrolysis of carbamide to yield ammonia and carbamic acid, which spontaneously decomposes into carbonic acid and second ammonia molecule [50]. Previous studies [51] have shown that carbon black (CB) and immobilized urease based biosensor exhibits three different actions, which depend on the applied CB electrode potential. At low potentials ($0 - 0.1$ V) of working electrode, one-electron electrochemical oxidation of carbamic acid can be monitored, meanwhile, at $0.2 - 0.5$ V electrode potentials, the electro-oxidation of carbamic acid and hydrazine were observed [51]. Thus, we assume that in our system, the principle of detection of carbamide is based on the direct carbamic acid oxidation (DCAO). As shown in Figure 8.1., urease catalyses the hydrolysis of carbamide to form carbamic acid and ammonia [50]. Electrochemical measurements were carried out by applying an electrode potential of 0.2 V at which the
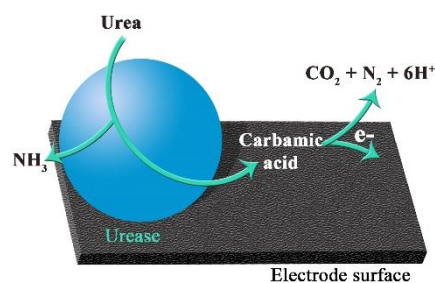

Fig. 3.8 *The principle of DCAO on carbonaceous materials surface, E = 0.2 V vs. Ag/AgCl.*

25

carbamic acid oxidizes by generating anodic current, correlating to carbamide concentration.

3.2.2.1 Examination of GOPs and TRGrO based systems

Aiming to test the ability for successful DCAO on the surface of synthesized materials, a set of biosensors with different carbonaceous materials has been designed. Primarily, the carbamide biosensors were designed by mechanically attaching and fixing membrane with immobilized urease on the surface of electrode containing GrO, GOPs, TRGrO or graphite (control biosensor). As in the PQQ-GDH case, the GrO based biosensor did not show any response to the substrate. DCAO were observed on the electrodes in all systems consisting GOPs, TRGrO and graphite. The kinetic parameters (j_{max}^{app} and K_M^{app}) and inactivation of biosensors are summarized in Fig. 3.9.
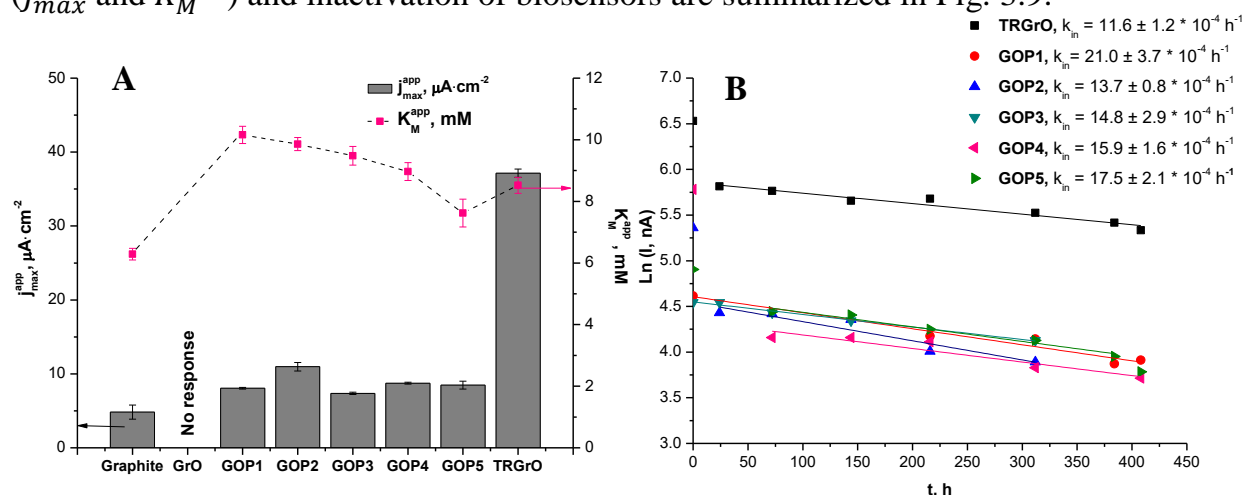

Fig. 3.9 *Kinetic characteristics (A) and stability (B) of carbamide biosensors based on immobilized urease on GOPs, TRGrO or graphite surface measured under standard conditions.*

From the graph above we can see that the highest DCAO efficiency exhibited biosensor using TRGrO as electrode material ($j_{max}^{app} = 37.1 \pm 0.6$ μA·cm^{-2}). This material has the highest S$_{BET}$ (235.8 ± 1.1 m^2·g^{-1}), the largest amount of the oxygen containing functional groups and the smallest size of particles ($d_{av} = 11$ nm, $h_{av} = 0.5$ nm) (Table 3.2) compared to GOPs and graphite. The lowest efficiency ($j_{max}^{app} = 4.8 \pm 1.0$ μA·cm^{-2}) of DCAO was observed on the surface of graphite containing electrode which was eight times lower compared to TRGrO contained biosensors. This DCAO action on the graphite surface shows that amount of oxygen containing functional groups doesn't play a crucial role in the DCAO on the surface of carbonaceous material. Nevertheless, j_{max}^{app} for others GOP1, GOP2, GOP3, GOP4 and GOP5 containing carbamide biosensors (8.1 ± 0.1, 11.0

± 0.6, 7.4 ± 0.2, 8.7 ± 0.1 and 8.5 ± 0.5 $\mu A \cdot cm^{-2}$, respectively) are higher compared to graphite based biosensor. The BET analysis reveals that S_{BET} of GOPs (7.6 ± 0.06 – 10.08 ± 0.06 $m^2 \cdot g^{-1}$) are smaller than graphite (13.1 ± 0.04 $m^2 \cdot g^{-1}$). These results suggest that electrode surface area also doesn't play crucial role in the DCAO. The AFM data shows that d_{av} of GOP$_S$ are smaller, while h_{av} of GOP$_S$ are higher than those of graphite (Table 3.2). The Raman spectroscopy data revealed that all GOPs have highest amount of defects compared to graphite (Fig. 3.1 B) and have basic functional groups on its surface (Table 3.1 and Fig. 3.1 A). The linear correlation between these characteristics of carbonaceous materials and j_{max}^{app} of biosensor was not found. For this reasons, we suggest that efficiency of DCAO on electrode surface depends not only on one characteristic of carbonaceous materials but it is influenced by the whole set of characteristics.

The carbamide biosensors based on all synthesized materials exhibited higher K_M^{app} value compared to that of native enzyme (1.8 mM [52]) (Fig. 3.9 A). Higher K_M^{app} values indicate a diffusion mode of action of the biosensor [21]. It was also observed (as in the PQQ-GDH case) that carbonaceous materials, obtained from the sonified graphite raw material (GOP2 and GOP4), exhibit lower K_M^{app} values in comparison with the samples, obtained using as-purchased graphite raw material. The clear correlation between K_M^{app} of biosensors and characteristics of carbonaceous materials also was not found.

The operational stability of the biosensors, designed using GOPs, TRGrO or graphite and urease, was investigated within 400 h. The responses to the 2.9 mM carbamide were periodically recorded at a working potential of 0.2 V in phosphate buffer solution. The inactivation data of biosensors are presented in Fig. 3.9 B. k_{in} for DCAO based carbamide biosensors were calculated. As can be seen in the Fig. 3.9 B, the inactivation process of carbamide biosensors with TRGrO, GOP2, GOP4 or GOP5 electrode materials can be divided into the faster (up to 24 h) and the slower steps (to 24 h). Faster inactivation process of biosensor can be attributed to leaching of the urease from the electrode surface between measurements. Meanwhile, sensitivity of GOP1 or GOP3 based biosensors decreases linearly beginning from the first measurement. The calculated k_{in} for different carbonaceous materials based biosensors were following: 21.0 ± 3.7·10^{-4} h^{-1} (GOP1), 13.7 ± 0.8·10^{-4} h^{-1} (GOP2), 14.8 ± 2.9·10^{-4} h^{-1}(GOP3), 15.9 ± 1.6·10^{-4} h^{-1}(GOP4), 17.5 ± 2.1·10^{-4} h^{-1} (GOP5) and 11.6 ± 1.2·10^{-4} h^{-1} (TRGrO). It is evident that the TRGrO based biosensor

exhibited the lowest k_{in} values, while the GOP based biosensor – the higher k_{in} values. The TGA and titrimetric analyses (Fig. 3.1 A and Table 3.1) revealed that TRGrO has the largest amount of the oxygen containing functional groups, while GOP1 has the lowest amount of the oxygen containing functional groups, which participate in DCAO. It has been reported that low concentrations of hydrophobic organic solvents unfold (process of denaturation) urease due to hydrophobic interaction [53]. This confirms our findings that the highest k_{in} value was obtained at the biosensor with the most hydrophobic surface – GOP1, while, the lowes k_{in} values was obtained at the biosensor with the most hydrophilic surface – TRGrO.

3.2.2.2 Examination of TRGO fractions based systems

Results obtained using PQQ-GDH or urease based biosensor showed (see chapters 3.2.1 and 3.2.2.1), that the TRGrO based systems exhibited the highest efficiency. Taking this into account, the new thermal reduction method of graphene oxide was proposed. This method allowed to separate and collect different fractions of thermally reduced graphene oxide (TRGO1, TRGO2 and TRGO3) with different physicochemical properties. The structural characteristics and surface morphologies of TRGO fractions have been evaluated (see chapter 3.1.2). Three different fractions of TRGO were tested as electrode materials for carbamide amperometric biosensors. The DCAO on the surface of electrode was achieved with all TRGO fractions. The dependence of the current density on carbamide concentration is shown in Fig. 3.10, where the inset presents the current-time responses to 3 mM of carbamide. The biosensors characteristics such as linear range, sensitivity, K_M^{app}, j_{max}^{app} and LOD are summarized in Table 3.5.
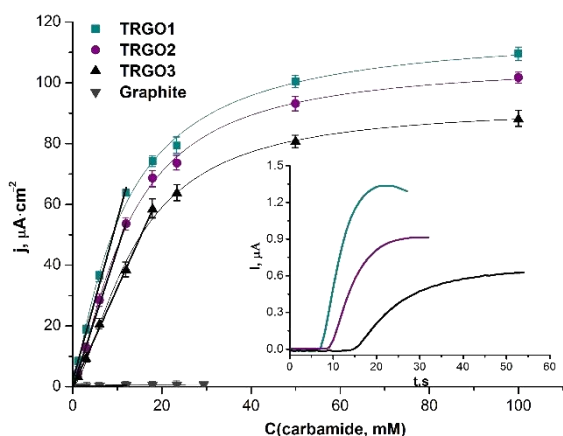

Fig. 3.10 *Dependence of steady-state current density (j) on carbamide concentration and linear part of curves measured under standard conditions, the inset shows current-time responses to 3.0 mM of carbamide.*

Table 3.4 *Characteristics of TRGO fractions and urease based carbamide biosensors.*

Biosensor material	Linear range, mM	Sensitivity, $\mu A \cdot mM^{-1} \cdot cm^{-2}$	R^2	K_M^{app}, mM	j_{max}^{app}, $\mu A \cdot cm^{-2}$	LOD, mM
Graphite rod	1.9 - 12.0	0.04 ± 0.002	0.9899	10.1 ± 0.5	0.89 ± 0.02	1.9
GO			No response			
TRGO1	0.26 - 12.0	5.4 ± 0.1	0.9907	11.4 ± 0.8	117.6 ± 3.5	0.26
TRGO2	0.15 - 12.0	4.5 ± 0.1	0.9976	12.3 ± 0.5	106.8 ± 1.91	0.15
TRGO3	0.15 - 17.9	3.3 ± 0.1	0.9900	13.8 ± 0.8	92.3 ± 2.7	0.15

From the data in Fig. 3.10 and Table 1 it can be seen that the TRGO1 based biosensor exhibits the highest DCAO effectivity (j_{max}^{app} = 117.6 ± 3.5 µA·cm^{-2}). The j_{max}^{app} of TRGO2 or TRGO3 based systems were lower (106.8 ± 1.9 and 92.3 ± 2.7 µA·cm^{-2} respectively). Nevertheless, the efficiencies of these biosensors were almost three times higher compared to TRGrO based biosensor, ten times higer compared to GOPs based biosensors and more than a hundred times higher than the control graphite rod biosensor (Fig. 3.9 A). The largest amount of the oxygen containing functional groups (Fig. 3.3) and the higher S$_{BET}$ of TRGO fractions compared to GOPs and TRGrO, could result in the higher efficiencies of DCAO. In our opinion, the crucial factor for efficiency of DCAO is the amount of oxygen-containing functional groups: TRGO1 S$_{BET}$ is one and a half time lower than that of TRGO3 and more than twice lower than that ofTRGO2 (Table 3.3), but this fraction has higher amount of oxygen functional groups compared to TRGO3 and TRGO2 (1.4 % and 1.2 %, respectively) (Fig. 3.3 inset). Considering this, DCAO can occur most effectively on this fraction surface. Other correlations between j_{max}^{app} and characteristics of TRGO fractions were not found.

Sensitivity of the biosensors was defined as the slope of the linear range of calibration curve (Fig. 3.10). The determined values of the sensitivity are higher than others carbamide biosensors, based on pH level measurements [54, 55] and the same order [56] or slightly lower [57] than carbamide biosensors, based on NH$_4^+$ selective electrode. It was observed that the LOD of carbamide for the TRGO1 based biosensors was 0.26 mM, for TRGO2 and TRGO3 based biosensors was 0.15 mM and for the control biosensor was 1.9 mM (Table 3.5).

The inset in Fig. 3.10 A compares the dynamics of the response for carbamide using different electrode materials. It is clearly seen that the biosensors have a different response time (Fig. 3.18 inset): 90 % of the steady-state current was achieved after 9.5 s, 11.4 s, 23.2 s and 56.0 s from the beginning of the bioelectrocatalysis process for the biosensors with TRGO1, TRGO2, TRGO3 and graphite, respectively. Thus, the highest reaction rate

is observed for the system with TRGO1 and the slowest - with graphite. These differences may indicate different mechanisms of catalysis determined by different surface characteristics of TRGO fractions. In our opinion, the main characteristics determining the highest rate of DCAO are the amount of oxygen-containing functional groups (which is able to facilitate the process of ET) and the structure of carbonaceous materials. Graphite has a crystalline structure, certain ordered structure exists in the case of TRGO2 and TRGO3, while amorphous structure prevails in the case of TRGO1 (XRD data; Fig. 3.5 A). In fact, the electrical conductivity of graphite is highly anisotropic [58], while amorphous carbon is completely isotropic [59]. These structural and electrical differences could result in ET rates through electrode materials to final acceptor. K_M^{app} values for bioelectrocatalytic systems with TRGO fractions and graphite (Table 3.4) confirm these suggestions. In general, higher K_M^{app} value in comparison to the value obtained in the solution of native enzyme (1.8 mM [52]) indicates that the significant diffusion barrier is between the sample and the reaction layer [21]. Meanwhile, the TRGO fractions based biosensors exhibited the higher K_M^{app} values compared to those of TRGrO or GOPs based biosensors (Table 3.4 and Fig. 3.9 A). This confirms a diffusion mode of action of the biosensor [21]. In our opinion, the largest amount of the defects (Fig. 3.5 B) and the higher S_{BET} (Table 3.3) of TRGO fractions compared to GOPs and TRGrO (Fig. 3.1 B and Table 3.2) results in higher diffusion barrier and K_M^{app} value.

The operational stability of the biosensors designed using TRGO fractions or graphite and urease are presented in Fig. 3.11.
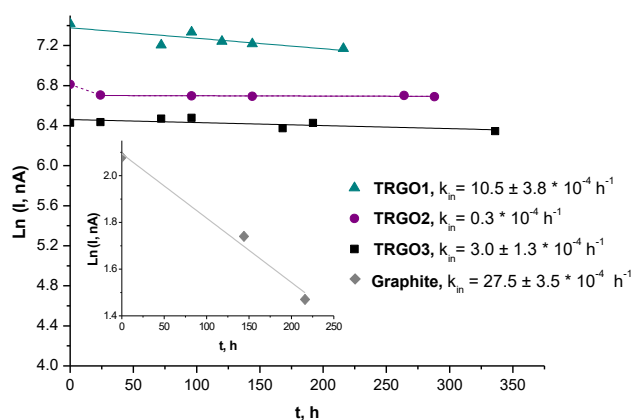

Fig. 3.11 S*tability of carbamide biosensors based on immobilized urease on TRGO fractions or graphite (inset) surface measured under standard conditions.*

The calculated k_{in} for different carbonaceous materials based biosensors were following: $10.5 \pm 3.7 \cdot 10^{-4}$ h^{-1} (TRGO1), $0.3 \cdot 10^{-4}$ h^{-1} (TRGO2), $3.03 \cdot 10^{-4}$ h^{-1} (TRGO3) and

$27.5 \pm 3.5 \cdot 10^{-4}$ h^{-1} (graphite). As can be seen the Fig. 3.11, the inactivation process of carbamide biosensors with TRGO2 electrode can be divided into the faster (up to 24 h) and the slower stages (to 24 h). Nevertheless, after 24 h, this biosensor exhibited the slowest inactivation process compared with other biosensors. Meanwhile, sensitivity of TRGO1 or TRGO2 materials based biosensors decreases linearly beginning with the first measurement. Graphite based biosensor exhibited the highest inactivation rate because the graphite is the most hydrophobic material and due to this the urease inactivation on this surface was more pronounced. In our opinion, the sensitivity of biosensors also decreased due to oxygen containing functional groups reduction during the experiment. In the literature [51] it was highlighted that hydrazine can be produced by the electro-oxidation reaction of carbamic acid. This compound is known as one of the best reducer of carbonaceous materials [26]. Thus, hydrazine can reduce the oxygen groups, which take part in the DCAO, on TRGO fractions surface, causing the sensitivity of biosensors to decrease.

3.2.3 Examination of TRGO fractions and FDH based reagentless systems

D-fructose is an important sugar widely used as a low-cost sweetener by the food and beverage manufacturers. It is widely distributed and can be found in fruit juices, honey, soft and energy drinks as well as in processed and diabetic food. Therefore, it is an important analyte in the food industry. However, excessive and prolonged consumption of D-fructose may lead to the development of metabolic disorders: renal and non-alcoholic fatty liver diseases, metabolic syndrome, obesity, diabetes and others [60 – 64]. Thus, this metabolite is also relevant for clinical diagnostics and has to be controlled in daily intake. It is obvious that that food quality control is essential both for consumer protection and for food industries. Conventional methods for D-fructose analysis are based on chromatography, spectrophotometry, electrophoresis and titration [65, 66]. Unfortunately, these methods do not allow an easy and rapid monitoring since they require relatively expensive instrumentation and well trained operators; moreover, they often include a time-consuming sample pre-treatment [67]. Therefore a vital step in food research, as well as in industry of medical devices for personal use is needed to develop a simple, fast and sensitive method for the determination of D-fructose.

Aiming to test the ability for successful DET between TRGO and FDH, a set of biosensors with different fractions of the TRGO, GO and unmodified graphite has been designed. The GO based biosensor did not show any response to the analyte. Unmodified graphite was used in the design of control electrode. DET was observed between the FDH and the electrode surface in all systems using TRGO fractions. The dependence of the current density on D-fructose concentration is shown in Fig. 3.12 where the insert presents the current-time responses to 2.2 mM of D-fructose. Main characteristics of the biosensors are summarized in Table 3.5.
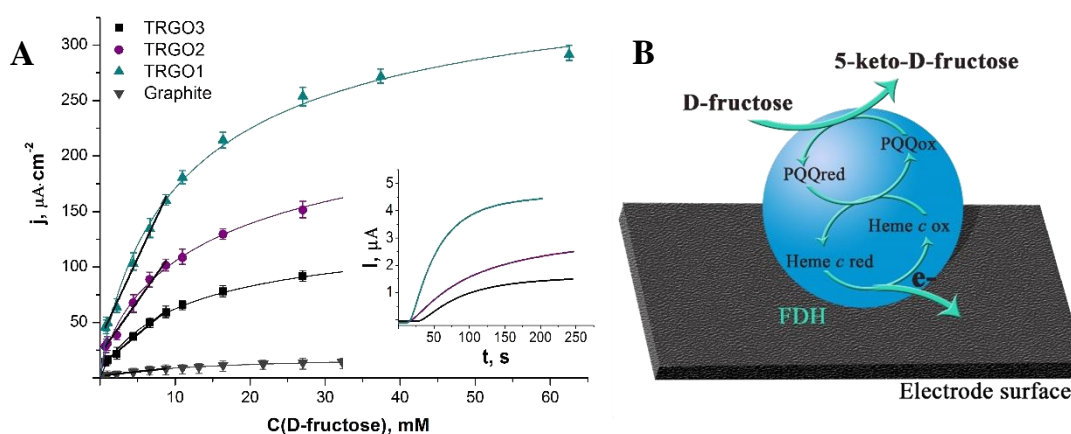

Fig. 3.12 *Dependence of steady-state current density (j) on D-fructose concentration and linear part of curves measured under standard conditions, the inset shows current-time responses to 2.2 mM of D-fructose (A). DET between active site of FDH and electrode using TRGO fractions, E = 0.4 V vs. Ag/AgCl (B).*

Table 3.5 *Characteristics of D-fructose biosensors.*

Biosensor materials	Linear range, mM	Sensitivity, $\mu A \cdot mM^{-1} \cdot cm^{-2}$	R^2	K_M^{app}, mM	j_{max}^{app}, $\mu A \cdot cm^{-2}$	LOD, mM
Graphite	0.7 – 8.8	0.7 ± 0.02	0.9952	15.1 ± 1.0	21.5 ± 0.6	0.7
GO			No responce			
TRGO1	0.7 – 8.8	14.5 ± 0.5	0.9947	9.5 ± 0.4	335.2 ± 6.1	0.7
TRGO2	0.7 – 8.8	9.5 ± 0.5	0.9937	12.9 ± 2.1	236.9 ± 14.4	0.7
TRGO3	0.6 – 8.8	5.7 ± 0.2	0.9949	10.1 ± 0.2	125.4 ± 1.2	0.6

As can be seen in Fig. 3.12 A, the DET was achieved in all systems. This effect is most probably due to that the FDH contains a heme *c*, which can act as an intrinsic electron transfer mediator. It is known that in a case of DET, the substrate D-fructose reacts with the PQQ of the FDH; further, the reduced cofactor reacts with the heme *c*, and finaly, the reduced heme *c* transfers the electrons to the electrode without the use of an additional external mediator. Schematically, the involvement of the enzymes in the DET can be represented as shown in a case of FDH in Figure 3.12 B. However, different TRGO fractions used in the role of electrode materials for D-fructose biosensors have developed different DET efficiency. The TRGO1 based system exhibited the highest sensitivity to

D-fructose while the TRGO3 using system was characterized by the lowest one (Table 3.5). The achieved high values of the sensitivity are the same order as for the other D-fructose sensors based on synergistic mediated processes (10 or 15 $\mu A \cdot mM^{-1} \cdot cm^{-2}$) [66, 68]. Obtained high current densities (Table 3.5) are beneficial not only for the bioanalytical purposes but also for the application of FDH-TRGO system in biofuel cells. Noteworthy that the sensitivity to D-fructose of biosensor based on unmodified graphite electrode was 10 times less, as compared with biosensors using TRGOs. It was observed that the LOD of D-fructose for the biosensors based on TRGO1, TRGO2 and TRGO3 were of 0.7 mM and for the graphite based biosensor was of 0.6 mM (Table 3.5).

It is known that the proper spatial orientation of the FDH on the electrode surface plays a crucial role for the direct heterogeneous electron transfer reactions [69]. Since the heme c is a hydrophobic moiety with a high affinity for adsorption on the electrode surface [70], this can affect the spatial orientation of the FDH. As can be seen in Fig. 3.12 A, the TRGO1 based system showed the highest DET sensitivity. The TGA and elemental analysis revealed that the TRGO1 has the largest amount of the oxygen containing functional groups that weigh significantly the orientation of enzyme and accelerate the ET from the active site of the FDH to the electrode. The surface of TRGO1, compared to that of TRGO2 and TRGO3, is the most hydrophilic due to the largest amount of oxygen-containing functional groups. Thus, when the nonionic surfactant Triton X-100 was used for the pretreatment of the biosensor electrode surface, the hydrophilic polyethylene oxide chains were directed toward the surface of TRGO1 while the lipophilic aromatic hydrocarbon groups were directed toward the opposite site. Taking into account the hydrophobic nature of the heme c, the FDH enzyme has to be properly situated on the surface pretreated with Triton X-100. Consequently, the biosensor based on TRGO1 fraction exhibited the highest sensitivity notwithstanding the lowest S_{BET} (Table 3.3).

The inset in Fig. 3.12 A compares the dynamics of the response for D-fructose using different electrode materials. It is clearly seen that the systems have a different response time: 90 % of the steady-state current was achieved after 100, 174 and 137 s from the start of the bioelectrocatalysis process for the biosensors using TRGO1, TRGO2 and TRGO3, respectively. Thus, the highest reaction rate is observed for the system with TRGO1; the slowest – with TRGO2. These differences may indicate different mechanisms of catalysis determined by different surface characteristics of TRGO fractions. This suggestion

confirms K_M^{app} values obtained for bioelectrocatalytic systems using TRGO fractions and graphite (Table 3.5). In general, higher value of K_M^{app} in comparison to the value of native enzyme obtained in solution (5 mM) [71] indicates that the significant diffusion barrier is present between the sample and the reaction layer [21]. The biosensor using TRGO2 exhibited slowest response and highest K_M^{app} value (12.9 mM) compared with graphite, TRGO1 and TRGO3. The BET analysis revealed that TRGO2 powder had the highest S_{BET} with the largest d_{av} of pore (Table 3.3). Supposedly, such size of pores led to the deep adsorbtion of FDH that complicates the diffusion of the substrate and the product to and from the active site of FDH and the surface of electrode. TRGO2 powder had the highest amount of defects (Raman spectra; Fig. 3.5 B) and the highest surface area (Table 3.3). However, it is obvious that the surface area does not play any crucial role in the efficiency of DET. The sensitivity data revealed that the highest DET rate was achieved between FDH and electrode surface using TRGO1 (Table 3.5). In our opinion, the crucial factor for the highest efficiency of DET was the relevant amount of oxygen-containing functional groups able to entail a proper spatial orientation of FDH. In that case, the ET in the operation of the biosensor with TRGO1 is not retarded by diffusion limits, as it is in the case of TRGO2. Moreover, the TRGO1 has a small concentration of defects, which facilitate electron transport in a single layer of graphene. The highest value of K_M^{app} (Table 3.5) was obtained in a case of bioelectrocatalytic system using graphite. The pristine graphite is characterized by the certain ordered structure (XRD data; Fig. 3.5 A), relatively high conductivity and small pore width. Supposedly, this crystalline structure without any functional groups is not favorable for proper FDH spatial orientation, which impedes the ET.

3.2.3.3 Stability of D-fructose biosensors

The operational stability of the biosensors was tested by consecutive measurements of the current response to a 4.4 mM D-fructose solution. Inactivation constants (k_{in}) for direct bioelectrocatalysis were calculated. The inactivation data of biosensors, based on adsorbed FDH on TRGO fractions surface, are presented in Figure 3.13 A
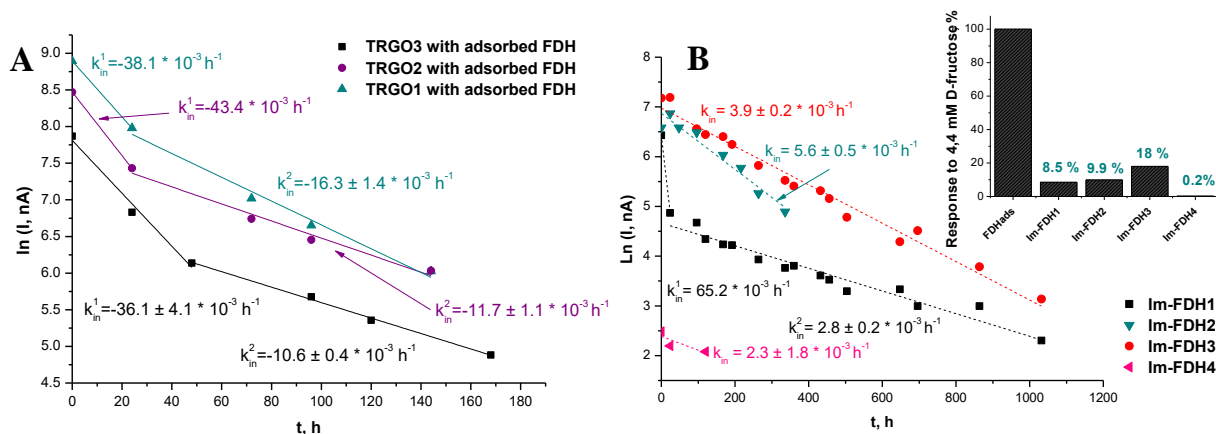
Fig. 3.13 *Stability of D-fructose biosensors, based on adsorbed FDH on TRGO fractions surface (A), and stability of different ways immobilized FDH on TRGO1 surface measured under standard conditions (B), the inset shows the sensitivity to 4.4 mM D-fructose obtained for each immobilization procedure first day after immobilization.*

As it can be seen from the Fig. 3.13, the inactivation process of D-fructose biosensors with different fractions of TRGO can be divided into the faster (k_{in}^1 from $36.1 \pm 4.1 \cdot 10^{-3}$ h^{-1} to $43.4 \cdot 10^{-3}$ h^{-1}) and the slower (k_{in}^2 from $10.6 \pm 0.4 \cdot 10^{-3}$ h^{-1} to $16.3 \pm 1.4 \cdot 10^{-3}$ h^{-1}) stages characterized by the different k_{in}. The TRGO3 based biosensor shows the highest stability. Nevertheless, after a period of 5 days, the sensitivity of all biosensors decreased by 90%. This result can be attributed to the thermal inactivation [71] and leaching of the FDH from the electrode surface between measurements at 20 ºC temperatures. Aiming to stabilise the operation of biosensor, the FDH was immobilized on the most sensitive electrode (TRGO1) of biosensor in four different ways: using BSA and glutar-aldehyde vapour (Im-FDH1), PEI and glutar-aldehyde vapuor (Im-FDH2), only glutar-aldehyde vapour (Im-FDH3) and poly(urethane-urea) (PUU) microparticles (Im-FDH4 – this immobilization was performed in VU ChGf Department of Polymer Chemistry).

The inactivation data of biosensors based on immobilized FDH on TRGO1 surface are presented in Fig. 3.13 B. These results suggest that in all cases of FDH immobilization, the biosensors stability increases from 3 to 7 times (k_{in} from $5.6 \pm 0.5 \cdot 10^{-3}$ h^{-1} to $2.3 \pm 1.8 \cdot 10^{-3}$ h^{-1}) campared to adsorbed FDH on TRGO1 surface ($k_{in}^2 = 16.3 \pm 1.4 \cdot 10^{-3}$ h^{-1}). Furthermore, inactivation processes of biosensors with imobilized FDH are characterized by one-stage. Nevertheless, it was found that FDH loses more than 80 % of the activity during immobilisation process in comparison to adsorbed FDH on TRGO1 surface (Fig. 3.13 B inset). In the Fig. 3.13 B inset we can see that the Im-FDH3 immobilized FDH had the highest residual activity (18 %). Moreover, after a period of 5 days, sensitivity of this

biosensor decreased by a less than 20 %. The obtained result should be considered as rather positive, comparable to that reported by Yabuki et al. [72], where the response magnitude after two hours from the preparation of the electrode became about the half of its initial value. The results on storage stability were reviewed by Bisccay et al. [66]. The best results showed that the biosensors can be stored approximately for 30 – 60 days, though, the storage temperature is −20 °C. Thus, we can conclude that the Im-FDH3 immobilized FDH and TRGO1 based biosensor displays a good stability and can be applied for D-fructose and D-tagatose determination.

3.3 Application of reagentless biosensors for analysis of real samples
3.3.1 Application of TRGO2 and urease based biosensor for detection of carbamide

Aiming to evaluate the concentration of carbamide in dialysate during HD procedure a new cabamide biosensor has been fabricated using TRGO2 and urease (see chapters 2.5 and 2.5.1). The new biosensor after addition of carbamide into electrochemical cell shows substrate-dependent anodic response. The response was measured as a difference between the steady state and the background current. The carbamide calibration curve with marked linear range and main characteristics of the biosensor are shown in Figure 3.14.
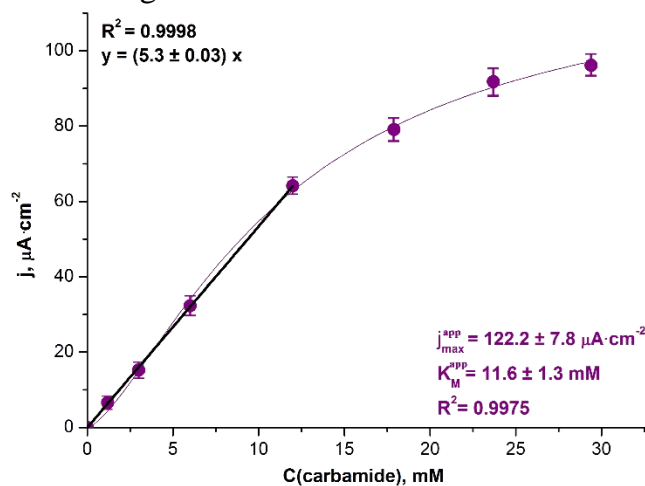

Fig. 3.14 *The carbamide calibration curve, the linear range (black line) and main characteristics obtained using the biosensor based on TRGO2 and urease measured under standard conditions.*

From the graph above we can see that characteristics of new biosensor (j_{max}^{app} = 122.2 ± 7.8 μA·cm^{-2}, K_M^{app} = 11.6 ± 1.3 mM, sensitivity – 5.3 ± 0.03 μA·mM^{-1}·cm^{-2} and linear range – up to 12.0 mM) are similar to those shown in Table 3.4. This show that we were able to reiterate production of biosensors.

The amperometric biosensor has been tested for carbamide measurements in dialysate as well. Aiming to validate responses of the biosensor measurements, the samples of dialysate in parallel were examined at the Vilnius University Hospital (VUH)

Santariskiu Clinics Laboratory of Biochemistry with ARCHITECT plus ic8200 (Abbott) analyzer. The testing has been carried out by investigating dialysate of eight patients during HD procedure. Data obtained by both methods are presented in Table 3.6.

Table 3.6 *Comparison of carbamide concentration obtained in dialysate using the amperometric biosensor and in the VUH Santariskiu Clinics Laboratory of Biochemistry.*

	Concentration of carbamide in dialisate, mM	
Nr.	Amperometric biosensor	VUH Laboratory of Biochemistry
1	5.4 ± 0.1	4.8
2	3.8 ± 0.3	3.8
3	3.2 ± 0.1	2.9
4	2.6 ± 0.3	2.7
5	6.8 ± 0.1	6.6
6	5.7 ± 0.1	5.7
7	3.8 ± 0.2	3.7
8	2.4 ± 0.1	2.3

The results obtained with the amperometric biosensor were plotted versus the results obtained in the VUH Laboratory of Biochemistry are presented in Figure 3.15.
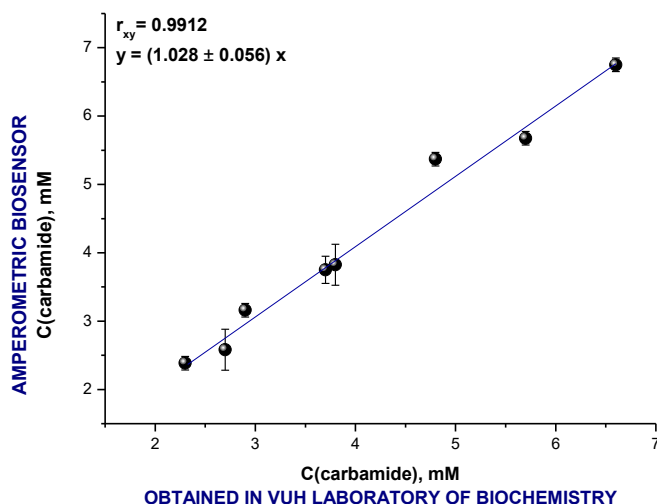

Fig. 3.15. *Correlation between carbamide concentration obtained in dialysate using the amperometric biosensor and in the VUH Santariskiu Clinics Laboratory of Biochemistry.*

As it can be seen from the data in Fig. 3.15, that the correlation coefficient (r_{xy}) between data obtained using biosensor and the data obtained in Laboratory of Biochemistry was 0.9912. This indicates excellent agreement between the two methods. The slope of the correlation was 1.028, indicating that the amperometric biosensor provided slightly higher results than those obtained in the VUH Santariskiu Clinics Laboratory of Biochemistry. These findings suggest that in general the biosensor based on TRGO2 and urease generate correct response to carbamide in dialisate during HD procedure.

3.3.2 Application of TRGO1 and FDH based biosensor for detection of D-fructose and D-tagatose

Primarily, the Im-FDH3 imobilized FDH and TRGO1 based biosensor have been tested for D-fructose measurements in fresh and heat treated apple and orange juices. For

this purpose, 5 µl of undiluted juices were added to the electrochemical cell containing 0.9 ml of buffer solution and the concentration of D-fructose was calculated using calibration curve. It was found that theses beverages contain of 16.3 ± 0.4 g/100 ml, 8.6 ± 0.3 g/100 ml, 13.7 ± 0.2 g/100 ml and 12.4 ± 0.2 g/100 ml of D-fructose, respectively. These results, showing that the proposed biosensor can be used for D-fructose measurements in popular beverages.

FDH is known as highly selective for D-fructose, but in this study we used this enzyme for D-tagatose detection. Evaluation of the total amount of D-tagatose in industrial products is very important for their quality. Also, it is very important for D-tagatose biosynthesis monitoring. Conventional methods for the D-tagatose analysis are based on chromatography [73] and spectrophotometry [74]. Unfortunately, these methods do not allow an easy and rapid monitoring, since they require relatively expensive instrumentation and well trained operators; moreover, they often include a time-consuming sample pre-treatment. Amperometric biosensors offer a promising alternative for the conventional methods. They have great potentials because of their high sensitivity, easier instrumentation, rapid (real-time) detection, low cost and ability to be used in turbid fluids with optically absorbing and fluorescing compounds. For this reason, amperometric biosensors are promising in development of simple and portable equipment.

D-tagatose is ketohexose having a structure similar to D-fructose, except for the orientation of the hydroxyl group on carbon 4 [75, 76]. Due to this reason, in this study we employ FDH as D-Tagatose biosensor recognition element. In this work we applied TRGO1 and immobilized FDH based amperometric biosensor for D-tagatose detection in D-galactose bioconversion into D-tagatose reaction mixture.

Reactor for synthesis of D-tagatose was designed using termophilic L-arabinose isomerase (TAI) from *Geobacillus lithuanicus 5* (obtained from VU GMC BchI Department of Molecular Microbiology and Biotechnology), which catalyses bioconvertion of D-galactose to D-tagatose. The production process of D-tagatose was carried out in thermostatically isolated reactor (volume 9 ml) at 50 °C in a stirred K-phosphate buffer solution (pH = 7.5) containing 444.4 mM D-galactose. TAI has been kept in dialysis bag in the middle of reactor. During biosynthesis, the samples were taken every 10 h until 50 h to determine the concentrations of D-tagatose.

Aiming to test the ability of FDH to catalyse the oxidation of D-tagatose to 5-keto-D-tagatose, FDH has been immobilized onto TRGO1 surface according to Im-FDH3 protocol. The responses of the manufactured biosensor to D-fructose and D-tagatose were measured as a difference between the steady state current and the background current. DET was observed between the FDH and the electrode surface in both cases. Dependences of experimentally measured steady-state currents on D-fructose and D-tagatose concentrations are presented in Fig. 3.16 A. Obtained dependences have been fitted by hypherbolic Michaelis-Menten eq. (1).
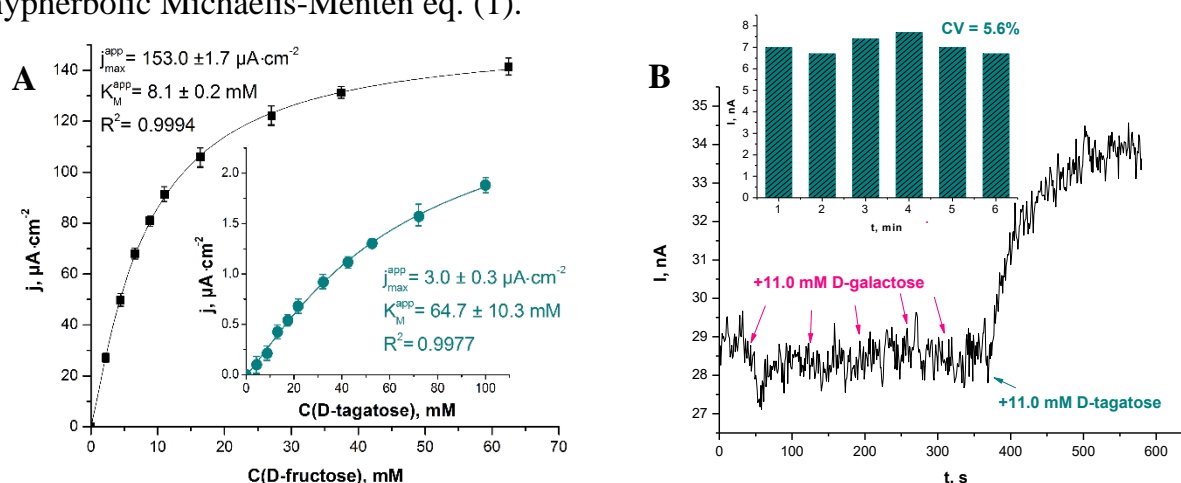

Fig. 3.16 *Dependences of steady-state current density on D-fructose and D-tagatose (inset) concentrations measured under standard conditions (A) and current time responses to D-galactose and D-tagatose, the inset shows signal reproducibility of biosensor to 11.0 mM D-tagatose in a stirred K-phosphate buffer solution of pH 7.5 (B).*

In the figure above we can see that the immobilized FDH onto TRGO1 surface catalyses D-fructose oxidation effectively ($j_{max}^{app} = 153.0 \pm 1.7$ µA·cm^{-2}), while the direct bioelectrocatalysis of D-tagatose by immobilized FDH is not very effective ($j_{max}^{app} = 3.0 \pm 0.3$ µA·cm^{-2}). Further analysis showed that the response to 4.4 mM D-tagatose in comparison with response to 4.4 mM D-fructose (which was taken as 100%.) is 0.33 ± 0.08 %.

It was determined, that the K_M^{app} value of D-tagatose biosensor was almost eight times higher than that of D-fructose. These results suggest that FHD, imobilised onto TRGO1 surface, binds the D-tagatose very weakly in comparison to D-fructose. Thus, determination of D-tagatose by biosensor, based on immobilized FDH onto TRGO1 surface is possible with the condition, that the analysis medium doesn't include D-fructose.

The purpose of the present study was to apply amperometric biosensor based on immobilized FDH onto TRGO1 surface, for D-tagatose detection in D-galactose

bioconversion into D-tagatose reaction mixture and to compare biosensor results with those obtained from spectrophotometric analyses. D-galactose bioconversion occurred in K-phosphate buffer solution of pH 7.5. In fact, optimal pH of the native FDH is 4.5 and any change of this pH value decreases its activity [71]. For this reason, we tested the sensitivity, selectivity and reproducibility of the signal of the biosensor in this medium. The changes of sensitivity were evaluated by measuring amperometric current time responses to 4.4 mM D-fructose and D-tagatose in McIlvaine buffer solution of pH 4.5 and in K-phosphate buffer solution of pH 7.5. A set of three biosensors designed in a same manner, was employed for the detection of D-fructose and D-tagatose in the same conditions. It was found, that residual activity of FDH to D-fructose in K-phosphate buffer solution is 37.84 ± 2.72 % (the responses to D-fructose in McIlvaine buffer solution was taken as 100%). Meanwhile, the response to D-tagatose in comparison with response to D-fructose (which was taken as 100 %.) in K-phosphate buffer solution is 1.93 ± 0.47 %. The presented results show, that the specificity of imobilised FDH to D-tagatose depends on the pH of the medium.

The selectivity of the prepared biosensor was studied toward determination of D-tagatose. For this purpose, the influence of D-galactose on the determination of D-tagatose was investigated. Fig 3.16 B. shows amperometric current time responses of the biosensor for D-tagatose in the presence of D-galactose in K-phosphate buffer solution.

As can be seen in Fig 3.16 B, no response is observed for biosensor in the presence of different concentrations of D-galactose. Meanwhile, the fast response of the biosensor towards D-tagatose can be achieved within hundreds of seconds after addition of D-tagatose. Furthermore, the biosensor response to D-tagatose did not changed after adding D-galactose. In order to check the reproducibility of biosensor signal a series of measurments in K-phosphate buffer solution were made for the detection of 11 mM D-tagatose within 300 min (Fig. 3.16 B inset). The relative standard deviation of the measurements of responses was of 5.6 %, which suggests a good reproducibility of the proposed electrode.

The adopted amperometric biosensor was applied for the analysis of D-galactose bioconversion into D-tagatose reaction mixture. Five samples of reaction mixture were analysed using standard addition method. The amounts of D-tagatose were obtained comparing the current time responses in the presence and in the absence of standard. D-

tagatose amount from two different measurements were averaged and summarized in Table 3.7. The same samples of reaction mixture were also analysed using the spectrophotometric analysis. The spectrophotometric analysis results of D-tagatose compared with results obtained using amperometric biosensor are presented in Table 3.7.

Table 3.7 *Comparison of the amount of D-tagatose, determined by using the amperometric biosensor and spectrophotometric analysis.*

	Amount of D-tagatose, mM	
t, h	Amperometric biosensor	Spectrophotometric analysis
0	0.0	0.0
10	36.3 ± 1.2	36.7
20	63.6 ± 3.8	54.3
30	81.7 ± 2.8	80.0
40	87.2 ± 6.4	92.9
50	93.5 ± 2.9	95.3

As can be seen in the Table 3.7, bioconversion reaction yield of 21 % was achieved at 50 h. The results obtained with the amperometric biosensor were plotted versus the results obtained with the spectrophotometric analysis and presented in Figure 3.17.
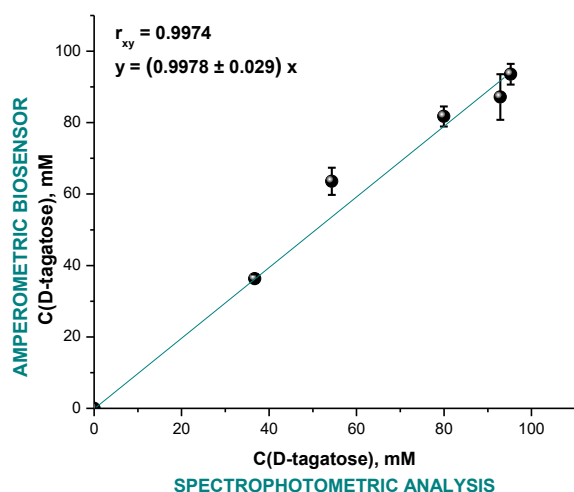

Fig. 3.17 *Correlation between amounts of D-tagatose, obtained by using the amperometric biosensor and spectrophotometric analysis in D-galactose bioconversion into D-tagatose reaction mixture.*

The correlation coefficient (r_{xy}) between biosensor and spectrophotometric analysis data of the same mixture was of 0.9974. This indicates excellent agreement between the two methods. The slope of the correlation was of 0.9978, which indicates, that results, determined using the amperometric biosensor, are slightly lower than those of spectrophotometric analysis. These findings suggest that, in general, the FDH and TRGO1 based biosensor generates correct response to D-tagatose in D-galactose bioconversion into D-tagatose reaction mixture.

4 CONCLUSIONS

1. Nine carbonaceous materials possessing beneficial properties towards direct electron transfer (DET) were synthesized using graphite oxidation by H_2O_2 or $K_3[Fe(CN)_6]$ in alkaline media (GOP(1 – 4)), enzymatic graphite oxidation by laccase from *Coriolopsis byrsina* (GOP5) or thermal reduction of graphite oxide (TRGrO) and by newly proposed thermal reduction and fractionalization system of graphene oxide (TRGO1, TRGO2, TRGO3).

2. The analysis of synthesized carbonaceous materials by eight different methods, reveald that all materials had included oxygen-containing functional groups which varied from 0.108 to 5.222 mmol·g^{-1} for GOP1 and GrO, respectively. Materials have different structures: GO – crystalline, while TRGO – amorphous but all of them were of nanometric size, which d_{av} ranges from 11 to 62 nm and h_{av} ranges from 0.5 to 5.5 nm for TRGrO and GOP3, respectively. The specific surface area of synthesized materials varied from 8.1 ± 0.03 to 689.5 ± 11.3 m²·g^{-1} for GOP1 and TRGO2, respectively. The concentration of defects (I(D)/I(G)) varied from 0.36 to 1.4 for GOP3 and TRGO2, respectively.

3. GOP(1 – 5), TRGrO and TRGO fractions were applicable for design of reagentless systems based on pyrroloquinoline quinone dependent glucose dehydrogenase from *Acinetobacter calcoaceticus* sp. (PQQ-GDH), urease from *Canavalia ensiformis* or D-fructose dehydrogenase from *Gluconobacter industrius* (FDH). Hovever, the thermally reduced materials based systems exhibited the highest efficiency of DET/DCAO expressed as j_{max}^{tar} (µA·cm^{-2}): 63.6 ± 5.8 (PQQ-GDH and TRGrO system), 117.6 ± 3.5 (urease and TRGO1 system), 335.2 ± 6.1 (FDH and TRGO1 system).

4. The examination of kinetic characteristics of new systems allowed to select the TRGrO and TRGO fractions as the most appropriate carbonaceous materials for reagentless D-glucose, carbamide and D-fructose biosensors design. The efficiencies of carbamide biosensors based on TRGO fractions were ten times higher compared to that of GOPs based biosensors and more than a hundred times higher than graphite based control biosensor. The sensitivity of D-fructose

biosensors is the same order as for the other synergistic mediated processes based systems.

5. The proposed biosensor based on urease and TRGO2 was applicable for precise detection of carbamide in dialysate. The correlation coefficient between data obtained in VUH Santariskiu Clinics Laboratory of Biochemistry and using the biosensor was of 0.9912.

The proposed biosensor based on FDH immobilized on TRGO1 by the method Im-FDH3 was applied for precise detection of D-tagatose in D-galactose bioconversion reaction mixture. The correlation coefficient between data obtained using the biosensor and the spectrophotometric analysis was of 0.9974.

5 LIST OF SCIENTIFIC WORKS
1.1 List of publications

1. J. Razumienė, V. Gurevičienė, M. Dagys, I. Šakinytė, A. Jonuška, L. Rimševičius, S. Marchenko, A. Soldatkin, Development of multi-parameter analyser based on electrochemical urea biosensors and electrolyte electrodes for monitoring of hemodialysis patients, 9th International Joint Conference on Biomedical Engineering Systems and Technologies, Biodevices proceedings (2016) 93 – 101 ISBN: 9789897581700.
2. M. Puida, J. Dabulytė-Bagdonavičienė, F. Ivanauskas, V. Razumas, J. Razumienė, I. Šakinytė, Glucose sensor based on nanostructured carbon electrode with immobilized PQQ-containing glucose dehydrogenase: Construction, experimental study and mathematical modeling, Nonlinear Analysis: Modelling and Control 21 (2016) 702 – 715.
3. I. Šakinytė, J. Barkauskas, J. Gaidukevič, J. Razumienė, Thermally reduced graphene oxide: the study and use for reagentless amperometric D-fructose biosensors, Talanta 144 (2015) 1096 – 1103.
4. J. Razumiene, I. Sakinyte, J. Barkauskas, R. Baronas, Nano-structured carbon materials for improved biosensing applications, Appl. Surf. Sci. 334 (2015) 185 – 191.
5. J. Razumiene, I. Sakinyte, V. Gureviciene, K. Petrauskas, Amperometric urea sensor enzyme immobilization into adjustable membrane and mathematical characterization of the biosensor, 8th International Conference on Biomedical Electronics and Devices, Biodevices, proceedings (2015) 144 – 149 ISBN: 978-989-758-071-0.
6. J. Razumiene, I. Sakinyte, V. Gureviciene, A. Jonuska, From carbon modification to analyzer design, IJEERT 5 (2015) special issue 19 – 24.
7. J. Razumienė, V. Gurevičienė, I. Sakinyte, J. Barkauskas, K. Petrauskas, R. Baronas, Modified SWCNTs for reagentless glucose biosensor: electrochemical and mathematical characterization, Electroanal. 25 (2013) 166 – 173.
8. J. Razumienė, I. Sakinyte, T. Kochane, S. Maciulyte, A. Straksys, S. Budriene, J. Barkauskas, Carbon electrode based urea sensor– modification of graphite and new polymeric carriers for enzyme immobilization, 6th International Joint Conference on Biomedical Engineering Systems and Technologies, Biodevices, proceedings (2013) 197 – 201 ISBN: 978–989–8565–34–1.
9. J. Barkauskas, J. Dakševič, S. Budrienė, J. Razumienė, I. Šakinytė, Adhesion of graphene oxide on a transparent PET substrate: a study focused on the optimization process, J. Adhes. Sci. Technol., 28 (2014), 2016 – 2031.

5.2 List of conferences thesis

International conferences:
1. J. Razumiene, I. Sakinyte, V. Gureviciene, J. Gaidukevic, Barkauskas J., Thermally reducated graphene oxide fractions for urea biosensor design: implementation and study, 150 th ICB Seminar, Micro and Nanosystems in biochemical Analysis, Program of the seminars, Poland, 2016 11 12 – 14, 22.
2. J. Razumienė, V. Gurevičienė, M. Dagys, I. Šakinytė, A. Jonuška, L. Rimševičius, S. Marchenko, A. Soldatkin, Development of multi-parameter analyser based on electrochemical urea biosensors and electrolyte electrodes for monitoring of

hemodialysis patients, 9th International Joint Conference on Biomedical Engineering Systems and Technologies, Biodevices, Italy, 2016 02 21 – 23, 42.

3. J. Barkauskas, J. Gaidukevič, J. Razumienė, I. Šakinytė, Electrocatalytic activity of graphene/(SCN)n composites for oxygen reduction reaction, Carbon'16: World Conference on Carbon, USA, 2016 07 10 – 15, 1 – 6.

4. J. Gaidukevič, J. Barkauskas, I. Šakinytė, J. Razumienė, Graphite oxide/(SCN)x Nanocomposite Materials: Synthesis, Characterization and Applications for ORR, 18th International Conference-School Advanced Materials and Technologies, Lithuania, 2016 08 27 – 31, 116.

5. J. Gaidukevič, J. Barkauskas, J. Razumienė, I. Šakinytė, R. Baronas, K. Petrauskas, Graphene/(SCN)n Composites as Efficient Electrocatalysts for the Oxygen Reduction Reaction, 3rd European Conference on Smart Inorganic Polymers, Portugal, 2016 09 12 – 14, 61.

6. J. Razumienė, V. Gurevičienė, M. Dagys, I. Šakinytė, A. Jonuška, L. Rimševičius, Applications of inexpensive and accurate biosensors in commercial analysers, Life Sciences Baltics 2016, Vilnius, Lithuania, 2016 09 14 – 17.

7. J. Razumiene, I. Sakinyte, V. Gureviciene, A. Jonuska. From Carbon Modification to Analyzer Design. Application of enzymes in bioelectrocatalytic systems. ICITSEM 2015 Proceedings of the Second International Conference on Innovative Trends in Science, Engineering and Management 2015, UAE, 2015 02 25 – 26, 78 – 81.

8. J. Barkauskas, J. Gaidukevič, J. Razumienė, I. Šakinytė, Synthesis and investigation of graphene-based parathiocyanogen nanocomposites, 2nd European Conference on Smart Inorganic Polymers: book of abstracts, USA, 2015 09 24 – 26, 43.

9. J. Razumiene, I. Sakinyte, V. Gureviciene, K. Petrauskas, Amperometric urea sensor enzyme immobilization into adjustable membrane and mathematical characterization of the biosensor, 8th International Conference on Biomedical Electronics and Devices, Biodevices, Portugal, 2015 01 12 – 15, 144.

10. I. Sakinyte, J. Razumiene, J. Barkauskas, J. Daksevic, Synthesis and characterization of sp^2 hybridized carbonaceous materials for D-(-)-tagatose biosensing, 2nd USA International Conference on Surfaces, Coatings and Nanostructured Materials (NANOSMAT-USA), USA, 2014 05 19 – 22, 118 – 119.

11. J. Razumiene, I. Sakinyte, R. Baronas, Nano-structurized carbon materials for improved biosensing applications, International Conference on Surfaces, Coatings and Nanostructured Materials (NANOSMAT-USA), USA, 2014 05 19 – 22, 178.

12. J. Barkauskas, J. Dakševič, E. Škikūnaitė, J. Razumienė, I. Šakinytė, Application of carbon nanomaterials in bioanalysis, The international and interdisciplinary conference "Nanotechnology: Research and Development, Lithuania, 2014 05 15 – 16, 37.

13. J. Razumienė, I. Šakinyte, T. Kochanė, S. Mačiulyte, A. Strakšys, S. Budrienė, J. Barkauskas, Modification of graphite and new polymeric carriers for enzyme immobilization, 6th International Joint Conference on Biomedical Engineering Systems and Technologies, Biodevices, Barselona, Ispanija, 2013 02 11 – 14, 30.

14. I. Šakinytė, J. Razumienė, J. Dakševič, J. Barkauskas, Graphite oxidation products: characterization and application, 5th International Symposium: Advanced micro- and mesoporous materials, Bulgaria, 2013 09 06 – 09, 79.

15. J. Razumienė, I. Šakinyte, V. Gurevičienė, B. Kurtinaitienė, A. Strakšys, T. Kochanė, S. Budriene, Polymeric carriers for immobilization of biocatalysts, 5th International Symposium: Advanced micro- and mesoporous materials, Bulgaria, 2013 09 06 – 09, 80.
16. S. Mačiulytė, G. Valungevičiutė, J. Razumienė, I. Šakinytė, T. Kochanė, I. Gerasimcik, S. Budrienė, Poly(urethane-urea) microcapsules for immobilization of maltogenase, Baltic Polymer Symposium 2013, Lithuania, 2013 09 18 – 21, 145.
17. A. Strakšys, A. Dulko, J. Razumienė, I. Šakinytė, T. Kochane, S. Budrienė, Immobilization and catalytic properties of maltogenic α-amylase on puu microparticles, Baltic Polymer Symposium 2013, Lithuania, 2013 09 18 – 21, 166.
18. I. Šakinytė, J. Razumienė, J. Barkauskas, Graphite oxidation products: synthesis, characterization and application, International conference of young chemists „Nanochemistry and Nanomaterials", Lithuania, 2012 12 07 – 09, 46.

National conferences:
1. Šakinytė, J. Razumienė, J. Barkauskas, J. Gaidukevič, Termiškai redukuoto grafeno oksido frakcijos: savybių studija ir taikymas efektyviai bioelektrokatalizei, penktoji jaunųjų mokslininkų konferencija „Fizinių ir technologijos mokslų tarpdalykiniai tyrimai", Lithuania, 2015 02 10, 31-32.
2. I. Šakinytė, J. Razumienė, J. Barkauskas, Grafito oksidacijos produktų sintezė, tyrimas ir taikymas bioelektrokatalizėje, Jaunųjų mokslininkų konferencija „Bioateitis: gamtos ir gyvybės mokslų perspektyvos", Lithuania, 2012 12 05, 16.

6 ACKNOWLEDGEMENTS

7 REFERENCES

1. S. Borgmann, A. Schulte, S. Neugebauer, W. Schuhmann, Amperometric Biosensors, in: R.C. Alkire, D.M. Kolb, J. Lipkowski (Eds.), Advances in Electrochemical Science and Engineering: Bioelectrochemistry, Wiley-VCH, Germany, 2011.
2. W. Putzbach, N.J. Ronkainen, Sensors 13 (2013) 4811 – 4840.
3. D. Grieshaber, R. MacKenzie, J. Vörös, E. Reimhult, Sensors 8 (2008) 1400 – 1458.
4. S. Viswanathan, H. Radecka, J. Radecki Monatsh. Chem. 140 (2009) 891 – 899.
5. P. Das, M. Das, S.R. Chinnadayyala, I.M. Singha, P. Goswam, Biosens. Bioelectron. 79 (2016), 386 – 397.
6. J. Wang, Analyst 130 (2005) 421 – 426.
7. B. Liang, L. Fang, G. Yang, Y. Hu, X. Guo, X. Ye, Biosens. Bioelectron. 43 (2013) 131 – 136.
8. Y. Shao, J. Wang, H. Wu, J. Liu, I.A. Aksay, Y. Lin, Electroanal. 22 (2010) 1027 – 1036.
9. A. Poulpiquet, A. Ciaccafava, E. Lojou, Electrochim. Acta 126 (2014) 104 – 114.
10. S. Wu, Q. He, C. Tan, Y. Wang, H. Zhang, Small (2013) 1 – 13.
11. T. Kuila, S. Bose, P. Khanra, A.K. Mishra, N.H. Kim, J.H. Lee, Biosens. Bioelectron. 26 (2011) 4637 – 4648.
12. J. Razumiene. A. Vilkanauskyte, V. Gureviciene, J. Barkauskas, R. Meskys, V. Laurinavicius, Electrochim. Acta 51 (2006) 5150 – 5156.
13. G. Brauer, Handbuch der Präparativen Anorganicshen Chemie. 3rd end., Ferdinand Enke verlang Stuttgort, Germany, 1975.
14. A.J.J. Olsthoorn, J.A. Duine, Arch. Biochem. Biophys. 336 (1996) 42 – 48.
15. L. Marcinkeviciene, R. Vidziunaitė, D. Tauraite, R. Rutkiene, I. Bachmatova, M. Morkunas, J. Razumiene, V. Casaite, R. Meskiene, J. Kulys, R. Meskys, Chemija 24 (2013) 48 – 58.
16. R.E. Wrolstad, T.E. Acerr, E.A. Decker, M.H. Penner, D.S. Reid, S.J. Schwartz, C.F. Shoemaker, D.M. Smith, P.Sporns, Common buffers and stock solutions, in: Current Protocols in Food Analytical Chemistry, John Wiley & Sons, Inc., 2001.
17. X. Yan, J. Chen, J.Yang, Q. Xue, P. Miele, ACS Appl. Mater. Interfaces 2 (2009) 2521 – 2529.
18. W.S. Hummers, R.E. Offeman, Am. Chem. Soc. 80 (1958) 1339 – 1339.
19. C.A. Leon, L.R. Radovic, Interfacial chemistry and electrochemistry of carbon surfaces. Chemistry and Physics of carbon, Marcel Dekker, New York, 1994.
20. M. Hosokawa, K. Nogi, M. Naito and T. Yokoyama, Nanoparticle Technology Handbook, Elsevier, Amsterdam, 2007.
21. F. Ivanauskas, I. Kaunietis, V. Laurinavičius, J. Razumienė, R. Šimkus, J. Math. Chem. 43 (2008) 1516 – 1526.
22. A. Turner, I. Karube, G.S. Wilson, Biosensors. Fundamentals and applications, Oxford Science Publications, New York, 1987.
23. D.R. Thvénot, K. Toth, R.A. Durst, G.S. Wilson, Biosens. Bioelectron. 16 (2001), 121 – 131.
24. F.D. Munteanu, A. Cavaco-Paulo, Anal. Lett. 43 (2010) 1126 – 1131.
25. A. Shrivastava, V.B. Gupta, Chron. Young Sci. 2 (2011) 21 – 25.

26. D.R. Dreyer, S. Park, C.W. Bielawski, R.S. Ruoff, Chem. Soc. Rev. 39 (2010) 228 – 240.
27. K. Haubner, J. Murawski, P. Olk, L.M. Eng, C. Ziegler, B. Adolphi, E. Jaehne, ChemPhysChem 11 (2010) 2131 – 2139.
28. W. Shen, Z. Li, Y. Liu, Rec. Pat. Chem. Eng. 1 (2008) 27 – 40.
29. R.J. Seresht, M. Jahanshahi, A.M. Rashidi, A.A. Ghoreyshi, Iran. J. Energy Environ.: Spec. Issue Nanotechnol. 4 (2013) 53 – 59.
30. Z. Ni, Y. Wang, T. Yu, Z. Shen, Nano Res. 1 (2008), 273–291.
31. A.C. Ferrari, J. Robertson, Phys. Rev. B 61 (2000) 14095 – 14107.
32. L.G. Cançado, M.A. Pimenta, B.R.A. Neves, M.S.S. Dantas, A. Jorio, Phys. Rev. Lett. 93 (2004) 247401: 1 – 4.
33. K.N. Kudin, B. Ozbas, H.C. Schniepp, R.K. Prud`homme, I.A. Aksay, R. Car, Nano lett. 8 (2008) 36 – 41.
34. J.M.C. Martin, G.B. Brieva, L.G. Fierro, Angew. Chem. Int. Ed. 45 (2006) 6962 – 6984.
35. V.P. Shilov, A.V. Gogolev, Russ. J. Gen. Chem. 79 (2009) 1773 – 1777.
36. C.G. Navarro, R.T. Weitz, A.M. Bittner, M. Scolari, A. Mews, M. Burghard, K. Kern, Nano Lett. 7 (2007) 3499 – 3503.
37. Z. Osvath, A. Darabont, P.N. Incze, E. Horvath, Z.E. Horvath, L.P. Biro, Carbon 45 (2007) 3022 – 3026.
38. A.B. Bourlinos, Th.A. Steriotis, M. Karakassides, Y. Sanakis, V. Tzitzios, C. Trapalis, E. Kouvelos, A. Stubos, Carbon 45 (2007) 852 – 857.
39. M. Thommes, Chem. Ing. Tech. 82 (2010) 1059 – 1073.
40. F. Guittonneau, A. Abdelouas, B. Grambow, S. Huclier, Ultrason. Sonochem. 17 (2010) 391 – 398.
41. C.H. Chuang, Y.F. Wang, Y.C. Shao, Y.C. Yeh, D.Y. Wang, C.W. Chen, J.W. Chiou, S.C. Ray, W.F. Pong, L. Zhang, J.F. Zhu, J.H. Guo, Sci. Rep. 4 (2014) 4525.
42. F.J. Hernandez, V.C. Ozalp, Biosensors 2 (2012) 1 – 14.
43. G. Srinivas, Y. Zhu, R. Piner, N. Skipper, M. Ellerby, R. Ruoff, Carbon 48 (2010) 630 – 635.
44. S. Park, R.S. Ruoff, Chemical methods for the production of graphenes,Nat. Nanotechnol. 4 (2009) 217 – 224.
45. T. Szabó, E. Tombácz, E. Illés, I. Dékány, Carbon 44 (2006) 537 – 545.
46. J. Razumienė, V. Gureviciene, E. Voitechovič, J. Barkauskas, V. Bukauskas, J. Nanosci. Nanotechnol. 11 (2011) 9003 – 9011.
47. A.A Karyakin, Bioelectrochemistry 88 (2012) 70 – 75.
48. P. Ramirez, N. Mano, R. Andreu, T. Ruzgas, A. Heller, L. Gorton, S. Shleev, Biochim. Biophys. Acta 1777 (2008) 1364 – 1369.
49. V. Laurinaviciusa, J. Razumienea, A. Ramanavicius, A. D. Ryabovc, Biosens. Bioelectron. 20 (2004) 1217 – 1222.
50. E.L.Carter, N. Flugga, J.L. Boer, S.B. Mulrooney, R.P. Hausinger, Metallomics 1 (2009) 207 – 221.
51. V. Laurinavicius, J. Razumiene, V. Gureviciene, IEEE Sens. J. 13 (2013) 2208 – 2213.
52. E.N. Danial, A.H. Hamza, R.H. Mahmoud, Braz. Arch. Biol. Technol. 58 (2015) 147 – 153.

53. F. Nabati, M. Habibi-Rezaei, M. Amanlou, A.A. Moosavi-Movahedi, J. Mol. Catal. B-Enzym. 70 (2011) 17 – 22.
54. A. Pizzariello, M. Stredanský, S. Stredanskà, S. Miertus, Talanta 54 (2001) 763 – 772.
55. I. Vostiar, J. Tkac, E. Sturdik, P. Gemeiner, Bioelectrochemistry 56 (2002) 113 – 115.
56. N. Stasyuk, O. Smutok, G. Gayda, B. Vus, Y. Koval'chuk, M. Gonchar, Biosens. Bioelectron. 37 (2012) 46 – 52.
57. M. Zhybaka, V. Beni, M.Y. Vagin, E. Dempsey, A.P.F. Turner, Y. Korpan, Biosen. Bioelectron. 77 (2016) 505 – 511.
58. N.J. Coville, S.D. Mhlanga, E.N. Nxumalo, A. Shaikjee, S. Afr. J. Sci. 107 (2011) 1 – 15.
59. NanoScienceWorks, Carbon allotropes, link: http://www.nanoscienceworks.org/nanopedia/carbon-allotropes, 2016 11 02.
60. V. Douard, R.P. Ferraris, J. Physiol. 291 (2013) 401 – 414.
61. V. Douard, A. Asgerally, Y. Sabbagh, S. Sugiura, S.A. Shapses, D. Casirola, R.P. Ferraris, J. Am. Soc. Nephrol. 21 (2010) 261 – 271.
62. S.E. Lakhan, A. Kirchgessner, Nutr. J. 12 (2013) 1 – -12.
63. M.F. Abdelmalek, A. Suzuki, C. Guy, A. Unalp-Arida, R. Colvin, R.J. Johnson, A.M. Diehl, Hepatology 51 (2010) 1961 – 1971.
64. M.J. Khandekar, P. Cohen, B.M. Spiegelman, Nat. Rev. Cancer 11 (2011) 886 – 95.
65. R. Antiochia, G. Vinci, L. Gorton, Food Chem. 140 (2013) 742 – 747.
66. J. Biscay, E.C. Rama, M.B.G. García, A.J. Reviejo, J.M.P. Carrazón, A.C. García, Talanta 88 (2012) 432 – 438.
67. R. Antiochia, L. Gorton, Sensor. Actuat. B-Chem. 195 (2014) 287 – 293.
68. S. Campuzano, R. Gálvez, M. Pedrero, F.J.M de Villena, J.M. Pingarrón, Anal. Bioanal. Chem. 377 (2003) 600 – 607.
69. M. Tominaga, C. Shirakihara, I. Taniguchi, J.Electroanal. Chem. 610 (2007) 1 – 8.
70. J. Tkáč, I. Voštiar, E. Šturdík, P. Gemeiner, V. Mastihuba, J. Annu, Anal. Chim. Acta 439 (2001) 39 – 46.
71. Toyobo Enzymes, D-fructose dehydrogenase from *glysonobactor sp.*, link: http://www.toyobo-global.com/seihin/xr/enzyme/pdf_files/093_096FCD_302.pdf, 2016 1102, FCD-302.
72. S. Yabuki, F. Mizutani, Electroanal. 9 (1997) 23 – 25.
73. P.M. Medeirosa, B.R.T. Simoneit, J. Chromatogr. A 1141 (2007) 271 – 278.
74. Z. Dische, J. Biol. Chem. 192 (1951) 583 – 587.
75. L.D. Grant, L.N. Bell, J. Food Sci. 77 (2012) C308 – 313.
76. G.V. Levin, J. Med. Food 5 (2002) 23 – 36.

8 REZUMĖ

Darbe siekta susintetinti, atrinkti ir ištirti sp² hibridizacijos anglines medžiagas ir jų pagrindu sukurti efektyviai veikiančias bereagentines fermentines sistemas. Anglinių medžiagų sintezei pasitelktos keturios skirtingos oksidacijos bei grafito ir grafeno oksidų terminės redukcijos metodikos. Gautos medžiagos charakterizuotos TGA, AJM, BET, SEM, XRD, Ramano sklaidos spektrinės, titrimetrinės ir elementinės analizės metodais. Ištirtos sp² hibridizacijos anglinės medžiagos buvo tiriamos kaip elektrodinės medžiagos amperometriniuose fermentiniuose biojutikliuose, kurių biologinę dalį sudarė PQQ-GDH, ureazė arba FDH. Geriausiomis savybėmis pasižymintys biojutikliai buvo atrinkti ir pritaikyti realių mėginių analizei.

Darbo išvados:.

1. Tiesioginei elektronų pernašai (TEP) tinkamomis savybėmis pasižyminčios devynios anglinės medžiagos susintetintos grafitą oksiduojant H_2O_2, $K_3[Fe(CN)_6]$ šarminėje terpėje (GOP(1 – 4)), veikiant fermentu lakaze išskirta iš *Coriolopsis byrsina* (GOP5), termiškai redukuojant grafito oksidą (TRGrO), naujai pasiūlytu terminės grafeno oksido redukcijos ir frakcionavimo metodu (TRGO1, TRGO2, TRGO3).

2. Aštuoniais metodais charakterizavus gautas anglines medžiagas nustatyta, kad visos turi deguoninių funkcinių grupių: atitinkamai GOP1 ir GrO nuo 0,108 iki 5,222 mmol·g⁻¹. Medžiagos turi skirtingą struktūrą – GO kristalinę, TRGO1 amorfinę struktūrą, tačiau visos yra sudarytos iš nanometrinės eilės dalelių, kurių d_{vid} kito nuo 11 iki 62 nm, o h_{vid} nuo 0,5 iki 5,5 nm (atitinkamai TRGrO ir GOP3). Medžiagų savitasis paviršiaus plotas kito nuo $8,1 \pm 0,03$ iki $689,5 \pm 11,3$ m²·g⁻¹ (atitinkamai GOP1 ir TRGO2), o defektiškumas (I(D)/I(G)) kito nuo 0,36 iki 1,4 (atitinkamai GOP3 ir TRGO2).

3. GOP(1 – 5), TRGrO ir TRGO frakcijos yra tinkamos bereagentinių sistemų kūrimui, kurių biologinę dalį sudaro nuo pirolo chinolinchinono priklausoma gliukozės dehidrogenazė išskirta iš *Acinetobacter calcoaceticus* sp. (PQQ-GDH), ureazė išskirta iš *Canavalia ensiformis* arba D-fruktozės dehidrogenazė išskirta iš *Gluconobacter industrius* (FDH), tačiau efektyviausiai TEP/TKRO išreikšta j_{max}^{tar} (µA·cm⁻²) vyko sistemose naudojant anglines medžiagas gautas terminės redukcijos būdu: $63,6 \pm 5,8$ (PQQ-GDH ir TRGrO); $117,6 \pm 3,5$ (ureazė ir TRGO1); $335,2 \pm 6,1$ (FDH ir TRGO1).

4. Įvertinus sukurtų sistemų kinetinius parametrus TRGrO ir TRGO frakcijos atrinktos kaip tinkamiausios anglinės medžiagos bereagentinių D-gliukozės, karbamido ir D-fruktozės biojutiklių kūrimui. Nustatytas karbamido biojutiklių efektyvumas yra dešimt kartų didesnis nei biojutiklių su GOP ir daugiau nei šimtą kartų didesnis nei kontrolinio biojutiklio su grafitu. D-fruktozės biojutiklių jautris yra tos pačios eilės, kaip ir mediatorinių sistemų.

5. Atrinktu biojutikliu su ureaze ir TRGO2 galima tiksliai įvertinti karbamido koncentraciją dializate. Nustatytas koreliacijos koeficientas tarp rezultatų gautų naudojant biojutiklį ir VUL Santariškių klinikų Biochemijos laboratorijos – 0,9912.

   Atrinktu ir pritaikytu biojutikliu su Im-FDH3 būdu imobilizuota FDH ir TRGO1 galima tiksliai įvertinti D-tagatozės koncentraciją biokonversijos iš D-galaktozės reakcijos mėginiuose. Nustatytas koreliacijos koeficientas tarp rezultatų gautų spektrofotometriniu metodu ir naudojant biojutiklį – 0,9974.

CURRICULUM VITAE

Name, Surname	Ieva Šakinytė
Birth date and pllace	6 September, 1988, Jurbarkas

Education

2012-2016	Doctoral degree studies at the Institute of Biochemistry of the Life Sciences Center at Vilnius University
2010-2012	Vilnius University Faculty of Chemistry, master degree in chemistry
2006-2010	Vilnius University Faculty of Chemistry, bachelor degree in chemistry
1994-2006	Graduation certificate of Eržvilkas secondary school

Work/practice experience

2017 01 tilll now	Junior research associate, Vilnius University, Life Sciences Center
2016 10-2016 12	Specialist, Vilnius University, Institute of Biochemisstry/ Life Sciences Center
2014 10-2016 4	Researcher, Vilnius University, Institute of Biochemisstry. This work has been supported by Lithuanian Agency for Science, Innovation and Technology Project E! 8835
2013 03-2014 09	Researcher, Vilnius University, Institute of Biochemisstry. This work was supported by Life Long Learning programme, Leonardo da Vinci, "Food Industry - Food Legislation, Impact Analysis, Training and Cooperation Network in Europe -E-Learning" 2012-1-TR1-LEO05-35116
2014 01-12	Junior research associate, Vilnius University, Institute of Biochemisstry. This work was funded by the European Social Fund under National Integrated Programme Biotechnology and Biopharmacy, grant VP1-3.1-SMM- 08-K01-005
2012 09-2013 12	Researcher, Vilnius University, Institute of Biochemisstry. This work was funded by the European Social Fund under National Integrated Programme Biotechnology and Biopharmacy, grant VP1-3.1-SMM- 08-K01-005
2010 07-2011 01	Engineer, Vilnius University, Institute of Biochemisstry. This work was supported by the Research Council of Lithuania grant "BIOSA" No.PBT-04/2010

Awards

2012	Laureate in the contest (best work of physical sciences) „Best Master's works of 2012 in Lithuania", organized by Lithuanian Society of Young researchers
2012	Wining an award for the best presentation at the national young scientific conference „Bioateitis: gamtos ir gyvybės mokslų perspektyvos", Vilnius
2011	Winning second place award at the national student scientific conference "Chemija ir cheminė technologija 2011", Kaunas

Contacts

Phone	+370 6017 9928
E-mail	sakinyte.ieva@gmail.com